AD-A061 133 RENSSELAER POLYTECHNIC INST TROY N Y COMMUNICATION A--ETC F/G 5/8
COMBINED SOURCE-CHANNEL CODING OF IMAGES.(U)
SEP 78 J W MODESTINO, D G DAUT N00014-75-C-0281
UNCLASSIFIED TR-78-1 NL

1 OF 1
AD
A061133

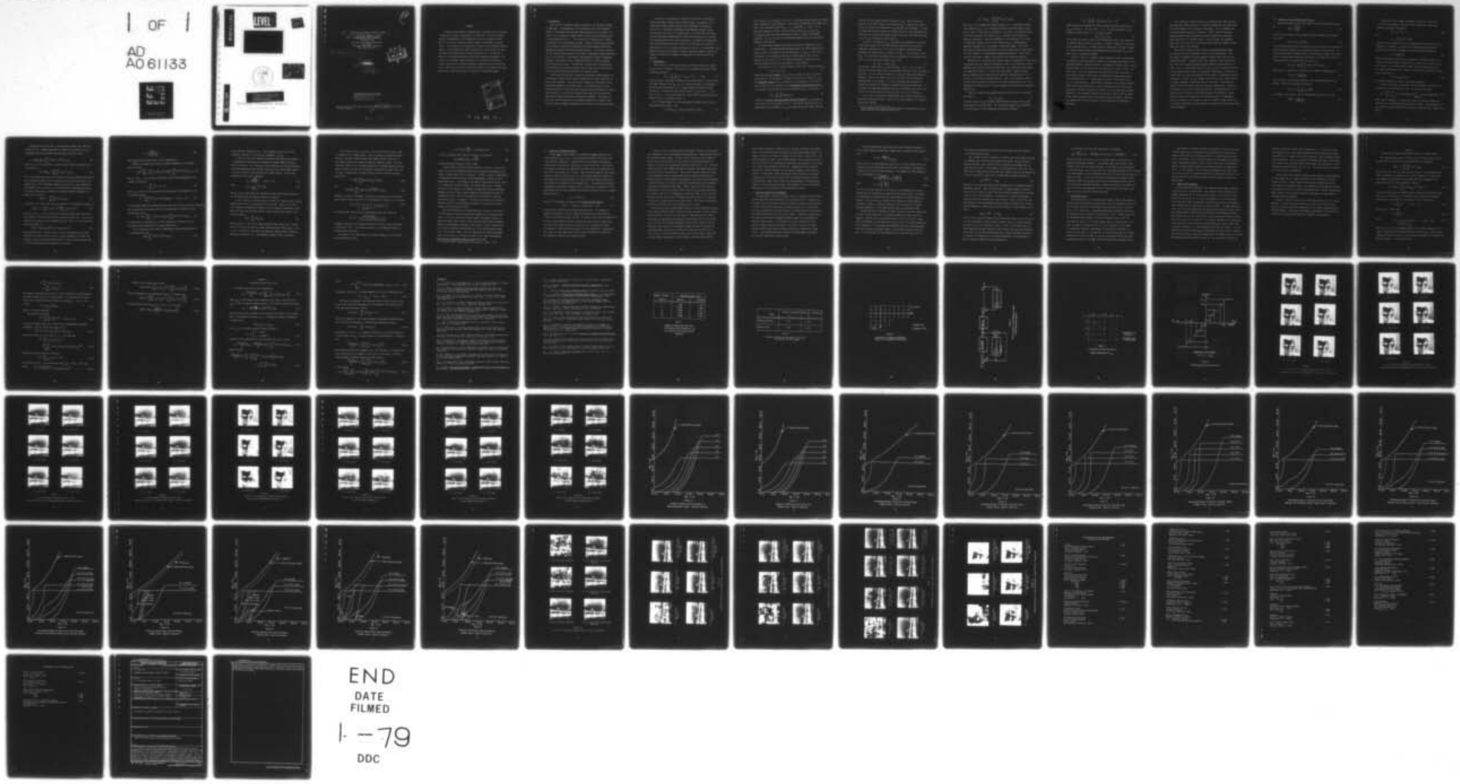

END
DATE
FILMED
1-79
DDC

(12)

(6)

# Combined Source-Channel Coding of Images

(10) J. W. Modestino [redacted] D. G. Daut
Communication and Information
Processing Group

Electrical and Systems Engineering
Department
Rensselaer Polytechnic Institute
Troy, New York 12181

(9) Technical rept.,

(14) TR-78-1

(11) Sep[redacted]78

(12) 71p.

This work was performed under Contract No. N00014-75-C-0281 for the Office
of Naval Research.

(15)

409 238

# ABSTRACT

A combined source-channel coding approach is described for the encoding, transmission and remote reconstruction of image data. The source encoder employs two-dimensional (2-D) differential pulse code modulation (DPCM). This is a relatively efficient encoding scheme in the absence of channel errors. In the presence of channel errors, however, the performance degrades rapidly. By providing error control protection to those encoded bits which contribute most significantly to image reconstruction, it is possible to minimize this degradation without sacrificing transmission bandwidth. The result is a relatively robust design which is reasonably insensitive to channel errors and yet provides performance approaching the rate-distortion bound. Analytical results are provided for assumed 2-D autoregressive image models while simulation results are described for real-world images.

## I. Introduction:

There has been widespread interest recently in the efficient encoding of image data. Two-dimensional (2-D) differential pulse code modulation (DPCM) is a technique which has been widely employed for this purpose. Its behavior in the absence of channel errors has been studied extensively and is well-documented [1]-[5]. In the presence of channel errors, however, the behavior of 2-D DPCM degrades rapidly. Indeed, on some fairly representative channels, increasing the quantization accuracy degrades rather than improves the subjective reconstructed image quality. As a result, some form of error control protection must be provided if high-quality image reconstruction is to be achieved. Since channel coding generally entails a bandwidth expansion, this operation can be extremely wasteful of channel bandwidth unless applied judiciously. In particular, tradeoffs must be made between the reconstruction accuracy associated with the source coder and the degree of error control protection provided by the channel coding.

In this paper we describe a combined source-channel coding approach for the encoding, transmission and remote reconstruction of image data which exploits these tradeoffs. The source encoder employs 2-D DPCM which has been appropriately matched to the image source. By providing selective error control protection to those bits which contribute most significantly to image reconstruction, it is possible to significantly improve the reconstructed image quality without sacrificing transmission bandwidth. The result is a relatively robust design which is reasonably insensitive to channel errors and yet provides performance approaching an achievable rate-distortion bound.

The overall 2-D DPCM system is described in Section II and includes typical performance results without channel coding. An analysis of the reconstructed output signal-to-noise ratio performance is provided in Section III. Theoretical performance bounds employing channel coding are described in Section IV. In particular, it is shown that these bounds indicate performance approaching the rate-distortion bound can be achieved with properly chosen error control protection. In Section V we demonstrate that these performance bounds are realistic in the sense that they can be approximated with a readily implemented class of convolutional codes. Simulation results are provided for typical real-world images in Section VI. Finally, in Section VII a summary and suggestions for future research are provided.

## II. Preliminaries:

While there are a wide range of possible stochastic models for images, we will restrict attention to the class of 2-D autoregressive random fields described according to

$$S_{i,j} = \sum_{k=0}^{K} \sum_{\ell=0}^{L}{}' a_{k,\ell} S_{i-k,j-\ell} + W_{i,j} \quad ; \quad i,j \geq 0 \tag{1}$$

where the prime is intended to indicate that the point $k=\ell=0$ is excluded from the double summation and $\{W_{i,j}\}$ is a 2-D zero-mean sequence of independent and identically distributed (i.i.d.) random variables possessing common variance $\sigma_w^2$. We assume that the initial values $S_{-k,-\ell}$ for $k=0,1, \ldots, K-1$ and $\ell = 0,1,\ldots, L-1$ have been specified. These initial values represent the boundary terms as illustrated in Fig. 1.

As a concrete example of a 2-D autoregressive process we note the 2-D Gauss-Markov random field. Here

$$S_{i,j}=\rho_1 S_{i-1,j} + \rho_2 S_{i,j-1} - \rho_1 \rho_2 S_{i-1,j-1} + W_{i,j} \tag{2}$$

with $0 \le |\rho_i| \le 1$, $i=1,2$ and $\{W_{i,j}\}$ a 2-D i.i.d. zero-mean Gaussian sequence possessing common variance $\sigma_w^2 = \sigma_s^2\,(1-\rho_1^2)(1-\rho_2^2)$. The quantity $\sigma_s^2$ represents the common variance of the resulting sequence $\{S_{i,j}\}$, i.e., $\sigma_s^2 = \mathrm{var}\{S_{i,j}\}$, $i,j \ge 1$. It is implicitly assumed, of course, that the initial values $S_{0,0}$, $S_{k,0}$ and $S_{0,\ell}$ for $1 \le k \le K$ and $1 \le \ell \le L$ have been appropriately chosen to result in stationary conditions. We will use this 2-D Gauss-Markov random field as an illustrative example in what follows.

An overall block diagram of the DPCM system under consideration is provided in Fig. 2. Following established nomenclature, the DPCM coding/decoding scheme is said to be matched to the message model if $\alpha_{i,j} = a_{i,j}$. That is, the coefficients in the feedback predictor are chosen equal to the 2-D autoregressive coefficients in (1). For analysis purposes we assume this to be the case although there may be good reason for other choices.

The notation of Fig. 2 deserves comment at this time. First the quantity

$$Y_{i,j} = S_{i,j} + Q_{i,j} \tag{3}$$

represents the <u>local estimate</u> of $S_{i,j}$ which is applied as input to the feedback predictor. In the absence of channel errors this is identical to $\hat{S}_{i,j}$ the <u>reproduced estimate</u> of $S_{i,j}$ released to the destination. The error incurred in this case is identical to the <u>instantaneous quantization error</u> $Q_{i,j}$. In the absence of quantization error and assuming $\alpha_{i,j} = a_{i,j}$, the quantity

$$\hat{S}^{+}_{i,j} = \sum_{k=0}^{K} \sum_{\ell=0}^{L}{}' \alpha_{k,\ell} Y_{i-k,j-\ell} \tag{4}$$

represent the <u>causal least mean-square predicted estimate</u> of $S_{i,j}$ making use of the data set as illustrated in Fig. 3. Note that in general due to the quantization errors inherent in $Y_{i,j}$, the quantity $\hat{S}^{+}_{i,j}$ will differ from the causal least mean-square predicted estimate of $S_{i,j}$. While it would be possible to use past[†] values of the sequence $\{S_{i,j}\}$ in making this prediction at the encoder, this information is unavailable at the decoder. In order to insure that both the encoder and decoder utilize the same information and thus avoid an otherwise potentially unstable situation, the encoder will make use of $\{Y_{i,j}\}$in forming the prediction $\hat{S}^{+}_{i,j}$.

In Fig. 2, the sequence $\{X_{i,j}\}$ represents the transmitted 2-D sequence whose values assume one of the $Q=2^n$ possible output levels of the n-bit quantizer. Exclusive use will be made of a symmetric uniform quantizer possessing the characteristic illustrated in Fig. 4. Note that $E_0=-\infty$ while $E_Q=\infty$. If $\Delta$ represents the uniform step size normalized to the standard deviation $\sigma_e$ of the input error sequence $\{E_{i,j}\}$ then

$$E_\ell - E_{\ell-1} = X_\ell - X_{\ell-1} = \Delta\sigma_e \tag{5}$$

The quantizer output level $X_\ell = [\ell-(Q-1)/2]\Delta\sigma_e$, $\ell=0,1,\ldots,Q-1$ is then expressed as an n-bit binary word for a subsequent transmission over the digital data link. In what follows we assume that a natural binary representation is employed. That is, the output level $X_\ell$ is coded into the natural binary representation of the integer $\ell$. It will be assumed that individual bit streams are available for subsequent modulation/coding and transmission. In particular, the modulation/coding is allowed to be different for each of the n serial bit streams associated with the output of the n-bit quantizer.

In all cases, the quantizer characteristics are chosen to minimize the mean-square quantization error. That is, the single parameter $\Delta$ is chosen to minimize the quantity

---

[†] In this context "past" values represent elements in the data set used for causal prediction as illustrated in Fig. 3.

$$\sigma_q^2 = E\{Q_{i,j}^2\} = \sum_{\ell=0}^{Q-1} \int_{E_\ell}^{E_{\ell+1}} [\xi - X_\ell]^2 \, p_E(\xi) d\xi \qquad (6)$$

where $p_E(\cdot)$ is the probability density function (p.d.f.) associated with the error sequence $\{E_{i,j}\}$. It is extremely difficult to provide explicit evaluation of $p_E(\cdot)$ in any realistic situation. As a result, we restrict attention to the two cases where the sequence $\{E_{i,j}\}$ is assumed either Gaussian or Laplacian distributed. From the experimental results provided in [6] there is substantial evidence that the error sequence $\{E_{i,j}\}$ is approximately Laplacian distributed for a wide-range of real-world images. For the 2-D Gauss-Markov random field described by (2), on the other hand, we would expect the error sequence to be approximately Gaussian distributed. The two cases considered then span a range of both practical and theoretical interest.

Tabulations of the optimum $\Delta$ for various number of quantization levels Q have been provided for the Gaussian distribution in Max [7], and likewise, for the Laplacian distribution in Paez and Glisson [8]. For convenience these results are summarized in Table 1. It should be noted, however, that the design approach employed here of optimizing the quantizer characteristics to minimize $\sigma_q^2$ is a decidedly suboptimum approach. That is, the quantizer characteristics should be chosen to minimize the overall reconstruction error. The mathematical intractability of the latter approach has influenced the approach adopted here.

Finally the sequence $\{R_{i,j}\}$appearing at the channel output is described according to

$$R_{i,j} = X_{i,j}+N_{i,j} \qquad (7)$$

where the sequence $\{N_{i,j}\}$ represents additive digital channel noise assumed independent from pixel-to-pixel. The reproducing estimate $\{\hat{S}_{i,j}\}$ delivered to the destination is then determined recursively according to

$$\hat{S}_{i,j} = \sum_{k=0}^{K} \sum_{\ell=0}^{L} \alpha_{k,\ell}\hat{S}_{i-k,j-\ell}+R_{i,j} \; ; \; i,j\geq 0 \tag{8}$$

again assuming that appropriate initial conditions have been specified for $\hat{S}_{-k,-\ell}$ for k=0,1,...,K-1 and $\ell$=0,1,...,L-1. As noted previously, in the absence of channel errors (i.e., $R_{i,j}=X_{i,j}$) we have

$$\hat{S}_{i,j} = S_{i,j} + Q_{i,j} \tag{9}$$

so that the only source of error is the quantization noise. The indexing of the channel output sequence $\{R_{i,j}\}$ must, of course, correspond to some established scanning pattern. In what follows we assume that the image is scanned in a fixed row-by-row raster scanning pattern and the sequence $\{R_{i,j}\}$ and hence $\{\hat{S}_{i,j}\}$ is ordered accordingly.

In Fig.'s 5 and 6 we illustrate typical behavior of this 2-D DPCM encoding scheme on a head-and-shoulders image for an optimum uniform Gaussian and Laplacian quantizer respectively both in the absence of channel errors. Corresponding results for an outdoor scene are illustrated in Fig.'s 7 and 8. The images here, as in the remainder of the paper, are all 256 x 256 arrays. These results assume a first-order 2-D autoregressive image model similar to that described by (2). In particular, the order of the predictor $\hat{S}^{+}_{i,j}$ in (4) is such that K=L=1. Least-squares estimates of the vertical and horizontal correlation coefficients, $\rho_1$ and $\rho_2$ respectively, were obtained and the predictor feedback coefficients set equal to the corresponding estimated quantities. The resulting estimates are provided in Table 2 and are typical of the values associated with a wide range of real-world images. These two test images will be used for purposes of illustration in the remainder of this paper.

In the absence of channel errors the 2-D DPCM encoding scheme provides reasonably good fidelity even for 1 bit/pixel although there are some distortions particularly in the vicinity of sharp edges. There is marginal subjective improvement beyond 2-3 bits/pixel. Results using the Laplacian quantizer provide barely perceptible subjective improvement indicating some insensitivity to quantizer choice. In what follows, all displayed images will be for the case of an optimum uniform Laplacian quantizer unless explicitly noted to the contrary.

The effects of channel errors on both the head-and-shoulders image and outdoor scene can be observed in Fig.'s 9 and 10 respectively. Here the channel is modeled as a binary symmetric channel (BSC) with bit error probability $P_b=10^{-3}$. Subjective tests have indicated a sharp threshold at this point with reconstructed image quality degrading rapidly beyond this point. This is indicated most clearly in Fig.'s 11 and 12 indicating results for the outdoor scene at $P_b=10^{-4}$ and $P_b=5\times10^{-3}$ respectively. The effects of channel errors are much more pronounced as the number of quantization levels Q increases. Indeed, for these channel error rates it would appear wasteful of channel bandwidth to employ more than 1-2 bits/pixel. Increasing the quantizer accuracy degrades rather than improves image quality. Similar results apply in the case of a Gaussian quantizer. The explanation for this behavior can be seen most clearly from the explicit evaluation of output signal-to-noise ratio provided in the following section. We demonstrate how, by a judicious use of channel coding, the subjective image quality can be improved substantially in the presence of channel noise without sacrificing channel bandwidth.

## III. Analysis of Output Signal-to-Noise Ratio:

The output signal-to-noise ratio ($SNR_0$) of the 2-D DPCM system is given by

$$SNR_0 = \frac{(\sigma_s^2/\sigma_e^2)}{e_T^2} \tag{10}$$

where $\sigma_s^2$ is the variance of the assumed zero-mean stationary 2-D sequence $\{S_{i,j}\}$ and

$$e_T^2 = E\{[S_{i,j}-\hat{S}_{i,j}]^2\}/\sigma_e^2 \tag{11}$$

is the resulting mean-square reconstruction error normalized to the variance $\sigma_e^2$ of the stationary sequence $\{E_{i,j}\}$ appearing as input to the quantizer. The quantity $(\sigma_s^2/\sigma_e^2)$ has an interpretation as the mean-square signal level normalized to the mean-square prediction error which, if we neglect the effects of quantization noise, is easily shown to be given by

$$(\sigma_s^2\,/\,\sigma_e^2) = (\frac{1}{2\pi})^2 \int_{-\pi}^{\pi}\int_{-\pi}^{\pi} |D(e^{j\lambda_1},e^{j\lambda_2})|^2 d\lambda_1 d\lambda_2 \tag{12}$$

Here $D(z_1,z_2)$ is defined as a function of the complex variables $z_1,z_2$ as

$$D(z_1,z_2) = \frac{1}{1-H(z_1,z_2)} \tag{13}$$

where $H(z_1,z_2)$ is the transfer function of the feedback predictor in the encoder. From (4) this quantity is given by

$$H(z_1,z_2) = \sum_{k=0}^{K}\ \sum_{\ell=0}^{L}{}' \ \alpha_{k,\ell} z_1^{-k} z_2^{-\ell} \tag{14}$$

For example, in the case of the 2-D Gauss-Markov process in (2) we have

$$\sigma_s^2/\sigma_e^2 = \frac{1}{(1-\rho_1^2)(1-\rho_2^2)} \tag{15}$$

Following a fairly standard development [9]-[12], the quantity $e_T^2$ in (10) can be expressed as the sum of three separate and conveniently normalized components according to

$$e_T^2 = \varepsilon_q + 2\varepsilon_m + \varepsilon_c \, . \tag{16}$$

Here,

$$\varepsilon_q = E\{Q_{i,j}^2\}/\sigma_e^2 = \sigma_q^2/\sigma_e^2$$

represents the mean-square value of the quantization noise normalized to $\sigma_e^2$. Similarly, the quantity $\varepsilon_c$ represents the normalized mean-square error contribution due solely to channel errors and evaluated according to

$$\varepsilon_c = E\{N_{i,j}'^{\,2}\}/\sigma_e^2 \tag{18}$$

where the stationary sequence $\{N_{i,j}'\}$ represents the additive noise at the output of the DPCM decoder in response to the channel noise sequence $\{N_{i,j}\}$ at its input. The system transfer function of the decoder $D(z_1,z_2)$ has been given previously by (13). Finally, the quantity $\varepsilon_m$ represents a mutual error term given by

$$\varepsilon_m = E\{Q_{i,j}N_{i,j}'\}/\sigma_e^2 \, . \tag{19}$$

We consider evaluation of each of these terms separately.

As stated previously, the quantizer has been designed to minimize the variance $\sigma_q^2$ of the quantization noise. It is easily shown that

$$\varepsilon_q = 2\sum_{\ell=1}^{Q/2-1}\int_{(\ell-1)\Delta}^{\ell\Delta}[y-(\ell-1/2)\Delta]^2\hat{p}_E(y)dy+2\int_{(Q/2-1)\Delta}^{\infty}[y-(Q-1)\Delta/2]^2\hat{p}_E(y)dy \tag{20}$$

where $\hat{p}_E(y) \triangleq \sigma_e p_E(\sigma_e y)$ is a normalized version of either the Gaussian or Laplacian p.d.f. possessing zero mean and unit variance. This expression for $\varepsilon_q$ is easily evaluated numerically for various values of $Q$ with $\Delta$ taken from Table 1.

Consider now the error term $\varepsilon_c$ contributed by channel error effects as defined by (18). Assuming again that the channel noise sequence $\{N_{i,j}\}$ is independent from pixel-to-pixel with mean-square value $e_n^2$ we have

$$\varepsilon_c = (e_n^2/\sigma_e^2)(\frac{1}{2\pi})^2 \int_{-\pi}^{\pi}\int_{-\pi}^{\pi} |D(e^{j\lambda_1}, e^{j\lambda_2})|^2 d\lambda_1\, d\lambda_2 \tag{21}$$

where $D(z_1,z_2)$ is the discrete 2-D system transfer function associated with the decoder and

$$e_n^2 = E\{N_{i,j}^2\} = \sum_{k=0}^{Q-1}\sum_{\ell=0}^{Q-1} (X_k - X_\ell)^2\, P_{k|\ell} P_\ell \quad . \tag{22}$$

This is merely the mean-square error incurred if $X_\ell$ was transmitted and decoded as the level $X_k$ averaged over the probability of all such error events. The quantity $P_{k|\ell}$ is the conditional probability that level $X_\ell$ was transmitted and decoded as level $X_k$ while $P_\ell$ is the probability of transmitting level $X_\ell$. It is more illuminating to consider the normalized quantity $e_n^2/\sigma_e^2$ which is easily seen to reduce to

$$e_n^2/\sigma_e^2 = \Delta^2 \sum_{k=0}^{Q-1}\sum_{\ell=0}^{Q-1} (k-\ell)^2\, P_{k|\ell}P_\ell \tag{23}$$

In Appendix A it is shown that this last quantity can be evaluated according to

$$e_n^2/\sigma_e^2 = \Delta^2\{\sum_{i=0}^{n-1} P_{b_i}(1-P_{b_i})2^{2i} + [\sum_{i=0}^{n-1} P_{b_i}(1-P_{b_i})2^i]^2\} \tag{24}$$

where $P_{b_i}$, $i=0,1,\ldots,n-1$ is the bit error probability associated with each of the successive bit positions in the n-bit quantizer output word. For the particular case of equal bit error probability $P_{b_i} = P_b$, $i=0,1,\ldots,n-1$ and this last expression reduces to

$$e_n^2/\sigma_e^2 = \Delta^2 P_b(1-P_b)\{(Q^2-1)/3 + P_b(1-P_b)(Q-1)^2\} \tag{25}$$

where we recall $Q=2^n$. In either case, the error contribution $\varepsilon_c$ is readily evaluated for various values of Q with $\Delta$ chosen from Table 1 for either the Gaussian or Laplacian quantizer characteristic. Again in the particular case of the 2-D Gauss-Markov process given by (2) we find

$$\varepsilon_c = \frac{e_n^2/\sigma_e^2}{(1-\rho_1^2)(1-\rho_2^2)} \tag{26}$$

with $e_n^2/\sigma_e^2$ given by either (24) or (25) as appropriate.

Finally, the mutual error term $\varepsilon_m$ is shown in Appendix B to be expressible in the form

$$\varepsilon_m = 2\Delta\Big[\sum_{\ell=Q/2}^{Q-1}\Big\{\sum_{i=0}^{n-1}(1-2\ell_i)P_{b_i}2^i\Big\}\varepsilon'_\ell\Big]\Big(\frac{1}{2\pi}\Big)^2\int_{-\pi}^{\pi}\int_{-\pi}^{\pi}D(e^{j\lambda_1},e^{j\lambda_2})\,d\lambda_1\,d\lambda_2\,. \tag{27}$$

Here $\ell_i$, $i=0,1,\ldots,n-1$ represent coefficients of the binary expansion of the integer $\ell$ according to

$$\ell = \sum_{i=0}^{n-1}\ell_i 2^i \;;\; \ell_i = 0,1 \tag{28}$$

while $P_{b_i}$ is the bit error probability associated with the transmission of the i'th bit and finally

$$\varepsilon'_\ell = \int_{E_\ell/\sigma_e}^{E_{\ell+1}/\sigma_e}\{y-[\ell-(Q-1)/2]\Delta\}\hat{p}_E(y)\,dy \quad ; \quad \ell=0,1,\ldots,Q-1 \tag{29}$$

is the average normalized quantization error given that the $\ell$'th level was transmitted. For the particular case where the bit error probability is constant for each bit position we have

$$\varepsilon_m = -4\Delta P_b\Big[\sum_{\ell=Q/2}^{Q-1}\{\ell-(Q-1)/2\}\varepsilon'_\ell\Big]\Big(\frac{1}{2\pi}\Big)^2\int_{-\pi}^{\pi}\int_{-\pi}^{\pi}D(e^{j\lambda_1},e^{j\lambda_2})\,d\lambda_1 d\lambda_2\,. \tag{30}$$

In either case, the quantity $\varepsilon_m$ is readily computed as a function of Q and the channel error probability for various image models.

For the particular case of the 2-D Gauss-Markov sequence described by (2) it is readily seen that

$$\Big(\frac{1}{2\pi}\Big)^2\int_{-\pi}^{\pi}\int_{-\pi}^{\pi}D(e^{j\lambda_1},e^{j\lambda_2})\,d\lambda_1 d\lambda_2 = 1 \tag{31}$$

which simplifies evaluation of $\varepsilon_m$. This component has been found to be negligible compared to the other error components $\varepsilon_q$ and $\varepsilon_c$.

In Fig.'s 13 and 14 we illustrate the behavior of $SNR_0$ for an assumed 2-D Gauss-Markov image model of the head-and-shoulders image and outdoor scene respectively. Here a Gaussian uniform quantizer was used and individual bits were transmitted using coherent binary phase-shift keyed (BPSK) modulation over an additive white Gaussian noise (AWGN) channel. The bit error probability in this case is given by

$$P_{b_i} = Q\left(\sqrt{\frac{2E_{si}}{N_0}}\right) \quad ; \quad i=0,1,\ldots,n-1 \tag{32}$$

where

$$Q(x) \triangleq \frac{1}{\sqrt{2\pi}} \int_x^{\infty} e^{-y^2/2} dy \tag{33}$$

and $E_{si}$ is the signal energy per transmitted binary channel symbol while $N_0/2$ is the double-sided noise spectral density in watts/Hz.

In these figures, the quantity $SNR_0$ is plotted as a function of the channel signal-to-noise ratio on a normalized per pixel basis. That is, if N uses of the channel are employed to transmit the n-bit quantizer output word corresponding to each pixel position then the channel signal-to-noise ratio is defined according to

$$SNR_i = \sum_{i=0}^{N-1} (2E_{si}/N_0) \tag{34}$$

where $E_{si}$, $i=0,1,\ldots,N-1$ is the signal energy for each channel use. Actually, in Fig.'s 13 and 14 N=n while we assume constant energy so that $E_{si}=E_s$ , $i=0,1,\ldots,n-1$. It will prove convenient when employing channel coding to allow the generality afforded by (34). The bandwidth expansion factor is then N/n.

Also included in Fig.'s 13 and 14 is the rate-distortion bound on $SNR_0$ for operation over an AWGN channel. This is obtained by equating the rate-distortion function, computed under a mean-square fidelity criterion, to the channel capacity and solving for $SNR_0$ as a function of $SNR_i$. The rate-distortion function for a continuous-amplitude 2-D Gaussian sequence has been given by Stuller and Kurz [13] following the development by Berger [14] in the 1-D case. In particular, the rate-distortion function R(D) has the parametric form

$$D = \left(\frac{1}{2\pi}\right)^2 \int_{-\pi}^{\pi}\int_{-\pi}^{\pi} \min\{\theta, S(\lambda_1,\lambda_2)\}\, d\lambda_1 d\lambda_2 \tag{35a}$$

and

$$R(D)=\left(\frac{1}{2\pi}\right)^2 \int_{-\pi}^{\pi}\int_{-\pi}^{\pi} \max\{0, \frac{1}{2}\log_2\frac{S(\lambda_1,\lambda_2)}{\theta}\}\, d\lambda_1 d\lambda_2 \tag{35b}$$

measured in units of bits/sample. Here $S(\lambda_1,\lambda_2)$ represents the 2-D discrete power spectral density which for a 2-D autoregressive process as in (1) becomes

$$S(\lambda_1,\lambda_2)=\left|\frac{1}{1-\sum_{k=0}^{K}\sum_{\ell=0}^{L}{}' a_{k,\ell}\, e^{-jk\lambda_1} e^{-j\ell\lambda_2}}\right|^2 . \tag{36}$$

In the particular case of the 2-D Gauss-Markov process this reduces to

$$S(\lambda_1,\lambda_2) = \frac{(1-\rho_1^2)(1-\rho_2^2)\sigma_s^2}{(1-2\rho_1\cos\lambda_1+\rho_1^2)(1-2\rho_2\cos\lambda_2+\rho_2^2)} . \tag{37}$$

A computer program for the numerical evaluation of R(D) has been constructed as described in [15]. In the present context, we have $SNR_0=\sigma_s^2/D$ where D is the mean-square distortion.

The capacity of the AWGN channel with signal energy $E_{si}$ is given by the well-known expression [16]

$$C = \frac{1}{2} \log_2[1+ \frac{2E_{si}}{N_0}] \quad \text{(bits/channel use)} \tag{38}$$

so that the maximum output SNR for N channel uses satisfies[†]

$$R(\sigma_s{}^2 SNR_0^{-1}) = \frac{N}{2} \log_2 [1+ \frac{SNR_i}{N}] \tag{39}$$

allowing solution for $SNR_0$ in terms of $SNR_i$.

Several things should be observed from Fig.'s 13 and 14. In the first place, note the sharp threshold effect which becomes more pronounced as the number of quantization levels Q increases. For $SNR_i$ in excess of approximately 20dB channel errors are rare and the performance is limited solely by quantization noise. An increase in the number of quantization levels results in a commensurate increase in $SNR_0$. For smaller $SNR_i$ we see a complete reversal of this behavior. For example, at $SNR_i$=12dB relative performance, measured in terms of $SNR_0$, actually improves by decreasing the number of quantization levels. This is an illustration of the behavior observed previously in Fig.'s 9 through 12. It should be noted that this threshold behavior occurs at error probabilities typical of that provided on many commercial and military data links.

The second observation to be made from Fig.'s 13 and 14 is that this 2-D DPCM scheme is relatively inefficient compared to the rate-distortion bound. In the next section we develop ultimate performance bounds to be achieved through channel coding. These bounds are based upon information-theoretic considerations and apply to all classes of codes. Results indicate relative performance arbitrarily close to the rate-distortion bound over a useful range of $SNR_i$. Later we demonstrate that these performance bounds are realistic in the sense that they can be closely approximated with an easily implemented class of convolutional codes.

[†] We assume constant signal energy so that $E_{si}=E_s$, $i=0,1,\ldots,N-1$.

## IV. Theoretical Performance Bounds:

A useful upper bound on $SNR_0$ can be obtained by lower bounding the bit error probability $P_{b_i}$, $i=1,2,\ldots,n-1$ associated with each of the bits in the n-bit quantizer output word. Consider first the case where the modulation/coding system treats each bit identically. Recall that N uses of the channel are required to transmit the quantizer output word so that the normalized code rate in bits per channel use is $R=n/N$. Under the AWGN assumption, the channel capacity is given by (38) with $E_{s_i} = E_s$, the constant energy per channel use. The converse to the coding theorem (cf. [16], [17]) then provides the desired lower bound on the common bit error probability $P_b$. Following the particularly illuminating development in McEliece [18], at rates above the capacity C of the AWGN channel, the bit error probability achievable by any rate R code is bounded away from zero by

$$P_b \geq H^{-1}(1-C/R) \tag{40}$$

where $H^{-1}(\cdot)$ represents the inverse of the binary entropy function

$$H(x) = -x\log_2 x - (1-x)\log_2(1-x) \; ; \quad 0<x<1 \tag{41}$$

At rates below capacity $P_b$ can be made negligibly small. For purposes of numerical evaluation, $P_b$ will be computed according to the right-hand side of (40) for $R>C$ and we set $P_b=0$ for $R\leq C$. It should be noted that this approach is similar to that employed by Chase et al.,[19] who observe that no known codes can achieve this lower bound on $P_b$ and even for $R<C$ infinitely long codes are required to achieve arbitrarily small bit error probability. Nevertheless, as we shall see, this bound does provide a useful perspective in assessing the efficacy of combined source-channel coding.

In Fig.'s 15-18 we illustrate typical performance results for the outdoor scene employing a fixed-rate modulation/coding approach. Similar results hold for the head-and-shoulders image. In each of these figures, the total number of channel uses is held fixed at the values N=2,3,4,5 respectively while the number of bits used in the quantizer assume the values n=1,2,...,N. Fixed-rate R=n/N codes then insure common transmission bandwidth requirements associated with all curves on the same figure. These curves indicate clearly the nature of the tradeoffs possible between quantization accuracy and sensitivity to channel errors at a fixed transmission bandwidth. The coded system performance is characterized by a reduction in saturation level $SNR_O$ but with a threshold occurring at significantly lower $SNR_i$. Indeed, the knee of this threshold characteristic occurs in all cases within 2-3dB of the rate-distortion bound. For example, from Fig. 15 if $SNR_O \geq 25$dB is required at $SNR_i$ as low as 5dB and allowing only two channel uses to transmit each pixel level a 1-bit quantizer is required in conjunction with a rate R=1/2 code. This level of performance could not be achieved with a 2-bit quantizer and no coding.

While the fixed-rate coding approach appears to offer performance approaching the rate-distortion bound, it should be noted that codes of fairly unusual rates like R=2/3, 3/4, 4/5, etc. are required. Relatively little is known concerning the construction and properties of practical codes of these rates. In Fig.'s 19-21 we illustrate performance bounds on $SNR_O$, again for the outdoor scene, when each bit in the quantizer output word can be accessed and separately coded. Attention is restricted to code rates of R=1/2,1/3,1/4 and 1/5 since a variety of practical codes exist at these rates. Again each of these figures corresponds to a fixed number of channel uses per pixel.

Error control protection is applied only to the most significant bit(s)(MSB) since errors here contribute most heavily to reconstructed image quality. For example, in Fig. 19 the number of channel uses per pixel is fixed at N=3. The several tradeoffs include a 3-bit uncoded system, a 2-bit system with a R=1/2 code on the MSB with the remaining bit unprotected, and finally a 1-bit system with a R=1/3 code employed on the only bit. Examination of these figures indicates the relative weakness of this approach compared to the fixed rate systems. In particular, unless some degree of error protection is applied to <u>all</u> bits of the quantizer output word, the threshold continues to exist at uncomfortably large values of $SNR_i$ and the performance is relatively poor compared to the rate-distortion bound. This behavior is due to the residual mean-square error contributions from unprotected bit errors.

## V. Practical Channel Code Performance:

The advantages of fixed rate channel coding in conjunction with 2-D DPCM source coding have been illustrated in the preceding section. Restriction to practical code rates, however, generally resulted in unequal error protection to each of the bits associated with a quantizer output word. Nevertheless, this latter approach can be quite effective in recovering most of the performance gains associated with the fixed rate scheme. It remains to demonstrate the degree to which these ultimate performance bounds can be approached by practical coding schemes. In particular, we restrict attention to short constraint length convolutional codes of rates R=1/2, 1/3 and 1/4 decoded using the Viterbi algorithm,an excellent description of which can be found in [20]. The optimum binary codes tabulated by Odenwalder[21] and Larsen [22] are used exclusively in what follows.

A useful exponentially tight bound on bit error probability obtained with Viterbi decoding on memoryless channels can be expressed in the general form

$$P_b \leq K_0 \left. \frac{dT(N,D)}{dN} \right|_{N=1, D=D_0} \tag{42}$$

where T(D,N) is the code generating function (cf. [20] for details) while the constants $K_0$ and $D_0$ depend upon the particular code employed, the modulation strategy in use and the channel parameters. For example, for BPSK modulation on the AWGN channel we have

$$K_0 \triangleq Q\left(\sqrt{\frac{2d_f RE_b}{N_0}}\right) \exp\left\{\frac{d_f RE_b}{N_0}\right\} \tag{43a}$$

while

$$D_0 = \exp\left\{-\frac{RE_b}{N_0}\right\} \tag{43b}$$

where $d_f$ is the free distance of the code, R is the normalized code rate in information bits transmitted per channel use and finally $E_b/N_0$ is the energy per information bit normalized to the single-sided noise spectral density $N_0$ watts/Hz. The quantity $E_b$ is related to the energy per channel symbol $E_s$ according to $E_s=RE_b$. A computer program has been developed [23] allowing numerical evaluation of this bound and thus explicit evaluation of $SNR_0$.

Typical results are illustrated in Fig.'s 22 for the case N=2 channel uses per pixel where optimum codes of constraint length K=3, 6 and 9 have been employed. Similar results are provided in Fig. 23 for the case N=3. These figures correspond to the optimum code results in Fig.'s 15 and 19 respectively. The convergence of the practical code performance toward the optimum performance with increasing constraint length K is illustrated clearly in Fig.'s 22 and 23. Unfortunately, the performance even for a K=9 code falls short of the optimum code performance by some 2-3dB and slightly more when compared to the rate-distortion bound.

Also included in Fig.'s 22 and 23 is a dotted curve labeled $R_0^*$ bound which is displaced some 2-3dB from the rate-distortion bound. We feel that this quantity provides a more realistic bound on achievable performance than the rate distortion bound. In particular, it is well-known (cf. [11], [24]) that there exists a block code of rate R and block length N such that the probability of error in decoding a source word of length K=NR is bounded according to:

$$P_e \leq 2^{-N[R_0-R]} \quad ; \quad R<R_0 \tag{44}$$

where $R_0$ is the so-called critical rate associated with the modulator/channel/demodulator cascade. Thus, for block codes, the single number $R_0$ provides a measure of both a range of rates R for which reliable communication is possible as well as the coding complexity, as reflected by N, required to guarantee a specified block-error probability. More recently, Viterbi [25] has shown for convolutional coding and maximum-likelihood sequence decoding on the constant, discrete memoryless channel that the error probability is upper bounded according to

$$P_e \leq C_R \, L \, 2^{-KR_0} \quad \text{if} \quad R<R_0, \tag{45}$$

where K is the constraint length of the convolutional code, R is the code rate, L is the total number of source letters encoded, and $C_R$ is a weakly dependent function of R and not a function of L and K. Thus, as with block codes, the single number $R_0$ provides a measure of both reliable rates and code complexity. Massey [26], [27] has used these observations to make an eloquent and persuasive argument for adopting $R_0$ as a modulator-demodulator design parameter in place of the more commonly used error probability.

As Wozencraft and Jacobs [24] demonstrate, the quantity

$$R_0^* = \frac{\log_2 e}{2}\left[1+E_s/N_0 - \sqrt{1+(E_s/N_0)^2}\right]+ \frac{1}{2}\log_2\left[\frac{1}{2}\left(1+ \sqrt{1+(E_s/N_0)^2}\right)\right] \qquad (46)$$

provides a useful upper bound on $R_0$ on the AWGN channel for any choice of modulator-demodulator parameters. The parameter $R_0^*<C$ then provides a more realistic limit than the channel capacity C on the range of rates achievable on the AWGN channel. In Fig.'s 22 and 23 the curve labeled $R_0^*$ bound then is obtained by equating $R_0^*$ to the rate-distortion function R(D) and solving for $SNR_0$ as a function of $SNR_i$. We see then that the use of practically implemented short constraint length convolutional codes results in performance within 1-2dB of the "practically achievable" $R_0^*$ bound. Similar conclusions can be drawn from Fig.'s 24 and 25 corresponding to N=4 and 5 channel uses respectively. Here results are shown only for practical K=6 codes.

## VI. Simulation Results:

The effectiveness of the combined source-channel coding scheme employing selected constraint length K=6 convolutional codes are illustrated in the case of the outdoor scene by the simulation results provided in Fig.'s 26-29 for N=2,3,4 and 5 respectively. Corresponding analytical performance evaluation is illustrated by the respective curves in Fig.'s 22-25. Similar results for the head-and-shoulders image in the case N=3 channel uses per pixel are illustrated in Fig. 30 . In all these figures, $SNR_i$ is constant across a row while the number of quantization bits n is held constant for each column. The transmission bandwidth requirements, as indicated by the number N of channel uses per pixel, is constant for all reconstructed images on a figure. Representative choices for $SNR_i$ in each case were made just below and above pronounced thresholds in the $SNR_0$ curves described in the preceding section.

These figures illustrate the dramatic improvements in subjective reconstructed image quality resulting from a judicious tradeoff between quantization accuracy and error control protection in a fixed transmission bandwidth. For example, in Fig. 28 we see clearly the advantages in allocating excess transmission bandwidth to error control rather than in attempting to improve the quantization accuracy by increasing the number of quantization levels. In this example, the 2-bit quantizer employing a K=6, R=1/2 code on each bit provides far superior reconstructed image quality than the 4-bit uncoded system or even the 3-bit system with error control protection on only the MSB.

## VII. Summary and Conclusions:

We have described an approach to the combined source-channel coding of a particular class of image sources. This approach offers theoretical performance approximating the rate distortion bound. We have shown how this theoretical performance can in turn by approximated by a class of practical short constraint length convolutional codes and demonstrated the performance gains through selected simulations on real-world images. The major deficiency lies in the lack of good high rate code constructions required to achieve the near optimum behavior indicated by the fixed-rate code performance results. More specifically, we have been forced to utilize previously tabulated optimum codes for rates R=1/2, 1/3 and 1/4. This severely compromises the flexibility of the approach in those situations where extremely high quality image reconstruction is required, i.e., high saturation level $SNR_0$ at low $SNR_i$. For more moderate reconstructed image quality requirements this restriction to available codes does not present a problem as demonstrated, for example, by Fig. 24 and the corresponding simulation results in Fig. 28. The result then, at least for moderate reconstructed image quality requirements, is a relatively robust design which offers a near optimum compromise between quantization accuracy and sensitivity to channel errors while preserving a fixed transmission bandwidth requirement. Work is in progress to determine and tabulate the properties of good short constraint length convolutional codes operating at the relatively high rates of $R=3/5$, $2/3$, $3/4$, etc. This should extend the flexibility of the approach considerably.

Another issue which deserves attention is the question of image modeling. We have assumed that the images of interest could be modeled as 2-D autoregressive models. Indeed, numerical results were provided only for the first-order 2-D Gauss-Markov model. The assumption of autoregressive behavior with Gaussian statistics is a gross oversimplification. Similar considerations apply, however, to more general stochastic image models and this aspect is presently under investigation.

Finally, it should be noted that we have made exclusive use of a uniform quantizer. This has certainly simplified the analysis but does raise the question of whether significant improvement can be realized through improved quantizer design. We feel that only marginal improvements can be expected by redesign of the quantizer although this question is being explored.

# Appendix A

## Evaluation of Normalized Mean-Square Error Due to Channel Noise

The normalized mean-square error due solely to channel noise is given by Eqn. (23) of the text which is repeated below for convenience

$$e_n^2/\sigma_e^2 = \Delta^2 \sum_{k=0}^{Q-1} \sum_{\ell=0}^{Q-1} (k-\ell)^2 P_{k|\ell} P_\ell \tag{A-1}$$

where each of the terms has previously been defined. By interchanging the order of summation, the summation on k is easily evaluated. In particular, this summation is recognized as the conditional mean of quantity $(k-\ell)^2$ given that the level $\ell$ was transmitted. That is,

$$E\{(k-\ell)^2|\ell\} = \sum_{k=0}^{Q-1} (k-\ell)^2 P_{k|\ell} = \overline{k^2} - 2\bar{k}\ell + \ell^2 \tag{A-2}$$

where, for convenience, the overbar indicates conditional expectation given the level $\ell$ was transmitted. We evaluate each of these terms separately. Consider first the quantity $\bar{k}$. The integer k can be expressed as

$$k = \sum_{i=0}^{n-1} k_i 2^i \quad ; \quad k=0,1,\ldots,Q-1 \tag{A-3}$$

where $k_i=0,1$. Observe that

$$\bar{k} = \sum_{i=0}^{n-1} \bar{k}_i \, 2^i \tag{A-4}$$

while

$$\begin{aligned} \bar{k}_i &= (1-P_{b_i})\ell_i + P_{b_i}(1-\ell_i) \quad ; \quad i=0,1,\ldots,N-1 \\ &= (1-2P_{b_i})\ell_i + P_{b_i} \end{aligned} \tag{A-5}$$

where $\ell_i=0,1$ is the corresponding element in the binary expansion of the integer $\ell$ representing the transmitted signal level and $P_{b_i}$ is the bit-error probability associated with the i'th bit which is allowed to be different for each bit position. It follows then that

$$\begin{aligned}\bar{k} &= \sum_{i=0}^{n-1} \{(1-2P_{b_i})\ell_i+P_{b_i}\}2^i \\ &= \ell + \sum_{i=0}^{n-1} (1-2\ell_i)P_{b_i}\, 2^i \quad .\end{aligned} \tag{A-6}$$

This shows, in particular, that there is a bias introduced in the declaration of channel output level due to channel errors. In the particular case when the bit error probabilities are all equal so that $P_{b_i}=P_b$ , $i=0,1,\ldots,N-1$, we have

$$\bar{k} = (1-2P_b)\ell + (Q-1)P_b \tag{A-7}$$

where it is recalled that $Q=2^n$.

Now consider the quantity

$$\overline{k^2} = \sum_{i=0}^{n-1}\sum_{j=0}^{n-1} \overline{k_i k_j}\, 2^{i+j} \quad ; \quad k=0,1,\ldots,Q-1 \tag{A-8}$$

If $i \neq j$ we have $\overline{k_i k_j} = \bar{k}_i \bar{k}_j$ since successive bit transmissions are assumed independent. For $i=j$, on the other hand, we have

$$\overline{k_i^2} = (1-P_{b_i})\ell_i^2 + P_{b_i}(1-\ell_i^2) = (1-2P_{b_i})\ell_i + P_{b_i} \tag{A-9}$$

where we have made use of the fact $\ell_i^2 = \ell_i$. It follows that

$$\begin{aligned}\overline{k^2} &= \sum_{i=0}^{n-1} \{(1-2P_{b_i})\ell_i+P_{b_i}\}2^{2i} \\ &+ \sum_{\substack{i=0 \\ i\neq j}}^{n-1}\sum_{j=0}^{n-1} \{(1-2P_{b_i})\ell_i+P_{b_i}\}\{(1-2P_{b_j})\ell_j+P_{b_j}\}2^{i+j} \quad ,\end{aligned} \tag{A-10}$$

whereupon after some algebra this reduces to

$$\overline{k^2} = \sum_{i=0}^{n-1} P_{b_i}(1-P_{b_i})\, 2^{2i} + \bar{k}^2 \tag{A-11}$$

with $\bar{k}$ given by (A-6). In the particular case $P_{b_i}=P_b$, $i=0,1,\ldots,N-1$, this yields

$$\overline{k^2} = \frac{P_b(1-P_b)(Q^2-1)}{3} + [(1-2P_b)\ell+(Q-1)P_b]^2 \quad . \tag{A-12}$$

Finally, in the general case we have

$$E\{(k-\ell)^2|\ell\} = \sum_{i=0}^{n-1} P_{b_i}(1-P_{b_i})2^{2i} + \left[\sum_{i=0}^{n-1} P_{b_i}(1-P_{b_i})2^{i}\right]^2 \tag{A-13}$$

which is independent of the transmitted level $\ell$. It follows that

$$e_n^2/\sigma_e^2 = \Delta^2\left\{\sum_{i=0}^{n-1} P_{b_i}(1-P_{b_i})2^{2i} + \left[\sum_{i=0}^{n-1} P_{b_i}(1-P_{b_i})2^{i}\right]^2\right\} \tag{A-14}$$

In the particular case that $P_{b_i} = P_b$, $i=0,1,\ldots,N-1$ we have

$$e_n^2/\sigma_e^2 = \Delta^2 P_b(1-P_b)\left\{\frac{(Q^2-1)}{3} + P_b(1-P_b)(Q-1)^2\right\} \tag{A-15}$$

# Appendix B

## Evaluation of Mutual Error Term

The mutual error term $\varepsilon_m$ can be expressed as

$$\varepsilon_m = \frac{E\{Q_{i,j}N'_{i,j}\}}{\sigma_e^2} = \sigma_e^{-2}\, E\left\{\sum_{k=-\infty}^{\infty}\ \sum_{\ell=-\infty}^{\infty} Q_{i,j}N_{k,\ell}d_{i-k,j-\ell}\right\} \tag{B-1}$$

where $\{N_{i,j}\}$ is the channel noise appearing at the input to the decoder and $\{d_{k,\ell}\}$ is the 2-D impulse response sequence of the decoder evaluated according to

$$d_{k,\ell} = \left(\frac{1}{2\pi j}\right)^2 \oint\!\!\oint D(z_1,z_2)z_1^{k-1}z_2^{\ell-1}dz_1dz_2 \tag{B-2}$$

with the closed contour integral taken around the unit polydisc in the complex space $\mathcal{C}^2$ possessing coordinates $z_1$, $z_2$. Assuming the channel is memoryless it follows that

$$E\{Q_{i,j}N_{k,\ell}\} = \delta_{i-k,j-\ell} \tag{B-3}$$

with $\delta_{i,j}$ the 2-D impulse sequence defined according to

$$\delta_{i,j} = \begin{cases} 1 & ; \quad i=j=0 \\ 0 & ; \quad \text{elsewhere} \quad . \end{cases} \tag{B-4}$$

Evaluation of the expectation on the right-hand side of (B-1) yields

$$\varepsilon_m = \frac{E\{Q_{i,j}N_{i,j}\}}{\sigma_e^2}d_{0,0} = \frac{E\{Q_{i,j}N_{i,j}\}}{\sigma_e^2}\left(\frac{1}{2\pi}\right)^2 \int_{-\pi}^{\pi}\int_{-\pi}^{\pi} D(e^{j\lambda_1},e^{j\lambda_2})d\lambda_1 d\lambda_2 \ . \tag{B-5}$$

Observe now that

$$\frac{E\{Q_{i,j}N_{i,j}\}}{\sigma_e^2} = \sigma_e^{-2}\sum_{k=0}^{Q-1}\ \sum_{\ell=0}^{Q-1}\left\{\int_{E_\ell}^{E_{\ell+1}} (\xi - X_\ell)p_E(\xi)d\xi\right\}(X_k - X_\ell)P_{k|\ell}$$

$$= \Delta \sum_{k=0}^{Q-1}\ \sum_{\ell=0}^{Q-1}(k-\ell)\varepsilon'_\ell P_{k|\ell} \tag{B-6}$$

where

$$\varepsilon'_\ell \triangleq \int_{E_\ell/\sigma_e}^{E_{\ell+1}/\sigma_e} \{y-[\ell-(Q-1)/2]\Delta\}\hat{p}_E(y)dy \ ; \ \ell=0,1,\ldots,Q-1 \ . \qquad \text{(B-7)}$$

Furthermore, since $\hat{p}_E(\cdot)$ is assumed symmetric it is easily established that

$$\varepsilon'_\ell = -\ \varepsilon'_{Q-1-\ell} \ ; \ \ \ell=0,1,\ldots,Q/2-1 \ . \qquad \text{(B-8)}$$

The sum on k appearing on the right-hand side of (B-6) is easily recognized as the conditional expectation of the difference $(k-\ell)$ given that the $\ell$'th level was transmitted. That is

$$E\{(k-\ell)|\ell\} = \sum_{k=0}^{Q-1} (k-\ell)P_{k|\ell} = \bar{k} - \ell \qquad \text{(B-9)}$$

where, as in Appendix A, the overbar indicates conditional expectation given the $\ell$'th level was transmitted. From previously established results

$$E\{(k-\ell)|\ell\} = \sum_{i=0}^{n-1} (1-2\ell_i)P_{b_i} 2^i \qquad \text{(B-10)}$$

where again $\ell_i$, $i=0,1,\ldots,n-1$ represent coefficients in the binary expansion of the integer $\ell$ and $P_{b_i}$ is the associated bit error probability. It follows that

$$\frac{E\{Q_{i,j}N_{i,j}\}}{\sigma_e^2} = \Delta \sum_{\ell=0}^{Q-1} \left\{ \sum_{i=0}^{n-1} (1-2\ell_i)P_{b_i} 2^i \right\} \varepsilon'_\ell \ . \qquad \text{(B-11)}$$

Now consider performing the summation on $\ell$. For each $\ell=0,1,\ldots,Q/2-1$ the term within braces will be the negative of that for the index $Q-1-\ell$. From the similar symmetry condition expressed by (B-8) we have

$$\frac{E\{Q_{i,j}N_{i,j}\}}{\sigma_e^2} = 2\Delta \sum_{\ell=Q/2}^{Q-1} \left\{ \sum_{i=0}^{n-1} (1-2\ell_i)P_{b_i} 2^i \right\} \varepsilon'_\ell \qquad \text{(B-12)}$$

so that finally

$$\varepsilon_m = 2\Delta \left[ \sum_{\ell=Q/2}^{Q-1} \left\{ \sum_{i=0}^{n-1} (1-2\ell_i)P_{b_i} 2^i \right\} \varepsilon'_\ell \right] \left(\frac{1}{2\pi}\right)^2 \int_{-\pi}^{\pi}\int_{-\pi}^{\pi} D(e^{j\lambda_1},e^{j\lambda_2})d\lambda_1 d\lambda_2 \ . \qquad \text{(B-13)}$$

## References

1. D. J. Connor, R. C. Brainard and J. O. Limb, "Intraframe Coding for Picture Transmission", Proceedings IEEE, vol. 60, pp. 779-791, July 1972.

2. J. B. O'Neal, "Predictive Quantizing System (Differential Pulse Code Modulation) for the Transmission of Television Signals", Bell Syst. Tech. J. vol. 45, pp. 689-721, May-June 1966.

3. D. J. Connor, R. F. W. Pease and W. G. Scholes, "Television Coding Using Two-Dimensional Spatial Prediction", Bell Syst. Tech. J., vol. 50, pp. 1049-1061, March 1971.

4. J. O. Limb and F. W. Mounts, "Digital Differential Quantizer for Television", Bell. Syst. Tech. J., vol. 48, pp. 2583-2599, September 1969.

5. J. O. Limb, C. R. Rubinstein and K. A. Walsh, "Digital Coding of Color Picturephone Signals by Element-Differential Quantization", IEEE Trans. Commun., vol. COM-19, pt. 1, pp. 992-1005, December 1971.

6. D. G. Daut, "An Empirical Study of Two-Dimensional Differential Pulse Code Modulation Encoding of Images", M. S. Thesis, Electrical and Systems Engineering Dept., Rensselaer Polytechnic Institute, Troy, N. Y., July 1977.

7. J. Max, "Quantizing for Minimum Distortion", IEEE Trans. Inform. Theory, vol. IT-6, pp. 7-12, March 1960.

8. M. D. Paez and T. H. Glisson, "Minimum Mean-Squared-Error Quantization in Speech PCM and DPCM Systems", IEEE Trans. Commun., vol. COM-20, pp. 225-230, April 1972.

9. R. E. Totty and G. C. Clark, "Reconstruction Error in Waveform Transmission", IEEE Trans. Inform. Theory, vol. IT-13, pp. 336-338, April 1967.

10. K.-Y. Chang and R. W. Donaldson, "Analysis, Optimization and Sensitivity Study of Differential PCM Systems Operating on Noisy Communications Channels", IEEE Trans. Commun., vol.. COM-20, pp. 338-350, June 1972.

11. J. E. Essman and P. A. Wintz, "The Effects of Channel Errors in DPCM Systems and Comparison with PCM Systems", IEEE Trans. Commun.,vol. COM-21, pp. 867-877, August 1973.

12. K.-Y. Chang and R. W. Donaldson, "Nonadaptive DPCM Transmission of Monochrome Pictures Over Noisy Communication Channels", IEEE Trans. Commun., vol. COM-24, pp. 173-183, February 1976.

13. J. A. Stuller and B. Kurz, "Intraframe Sequential Picture Coding", IEEE Trans. Commun.,vol. COM-25, pp. 485-495, May 1977.

14. T. Berger, Rate Distortion Theory: A Mathematical Basis for Data Compression, Prentice-Hall, Englewood Cliffs, N.J., 1971.

15. D. G. Daut, "Rate-Distortion Function for 2-D Image Model", unpublished R.P.I. report, April 1978.

16. R. G. Gallager, Information Theory and Reliable Communication, Wiley, New York, 1968.

17. F. Jelinek, Probabilistic Information Theory, McGraw-Hill, New York, 1968.

18. R. J. McEliece, The Theory of Information and Coding, vol. 3, Encyclopedia of Mathematics and Its Applications, Addison-Wesley, Reading, Mass., 1977.

19. D. Chase, et al.,"Multi-Sample Error Protection Modulation Study", TR-76-161, Rome Air Development Center, Air Force Systems Command, Griffiss Air Force Base, New York, May 1976.

20. A. J. Viterbi, "Convolutional Codes and Their Performance in Communication Systems", IEEE Trans. Commun., COM-19, pp. 751-772, October 1971.

21. J. P. Odenwalder, "Optimum Decoding of Convolutional Codes", Ph.D. Dissertation, Syst. Sci. Dept., Univ. California, Los Angeles, 1970.

22. K. J. Larsen, "Short Convolutional Codes with Maximal Free Distance for Rates 1/2, 1/3, and 1/4", IEEE Trans. Inform. Theory, vol. IT-19, pp. 371-372, May 1973.

23. J. W. Modestino, "Evaluation and Graphical Display of Performance of Viterbi Decoder in Conjunction with Coherent BPSK Modulation on AWGN Channel", TM78-3, Electrical and Systems Engineering Department, Rensselaer Polytechnic Institute, Troy, N. Y., January 1978.

24. J. M. Wozencraft and I. M. Jacobs, Principles of Communications Engineering, Wiley, New York, 1965.

25. A. J. Viterbi, "Error Bounds for Convolutional Codes and an Asymptotically Optimum Decoding Algorithm", IEEE Trans. Inform. Theory, vol. IT-13, pp. 260-269, April 1967.

26. J. L. Massey, "Coding and Modulation in Digital Communications", Proc. Int. Zurich Seminar on Digital Communications, Zurich, Switzerland, March 1974.

27. J. L. Massey, Course Notes for EE453, Dept. of Elect. Eng., Univ. of Notre Dame, Indiana, 1976.

| Number of Output | Normalized Step Size Δ | |
|---|---|---|
| Levels Q | Gaussian | Laplacian |
| 2 | 1.596 | 1.414 |
| 4 | 0.996 | 1.087 |
| 8 | 0.586 | 0.731 |
| 16 | 0.335 | 0.456 |
| 32 | 0.1881 | 0.281 |

Table 1

Summary of Normalized Step Size Δ
for Optimum Uniform Quantizers for
both Gaussian and Laplacian Error
Sequences

| Image | Vertical Correlation $\rho_1$ | Horizontal Correlation $\rho_2$ |
|---|---|---|
| Head-and-Shoulders | 0.973 | 0.981 |
| Outdoor Scene | 0.957 | 0.967 |

Table 2

Estimated Vertical and Horizontal Correlation Coefficients for Test Images

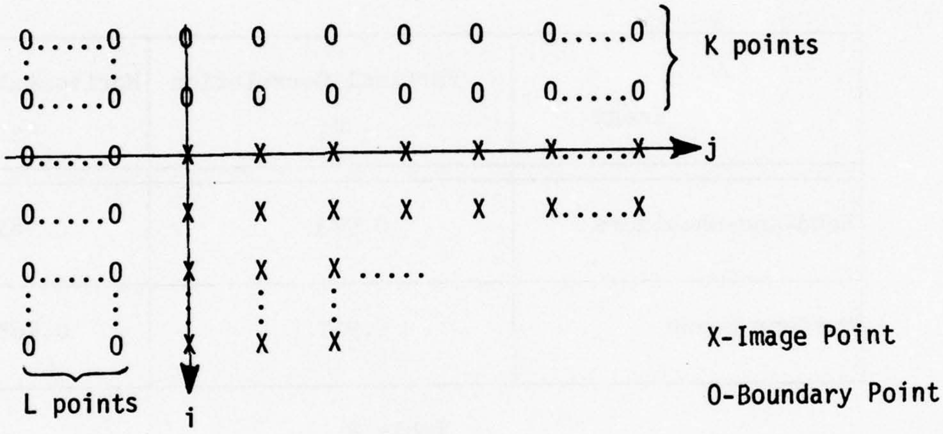

Figure 1

Illustration of Image and Boundary Points in 2-D Autoregressive Process

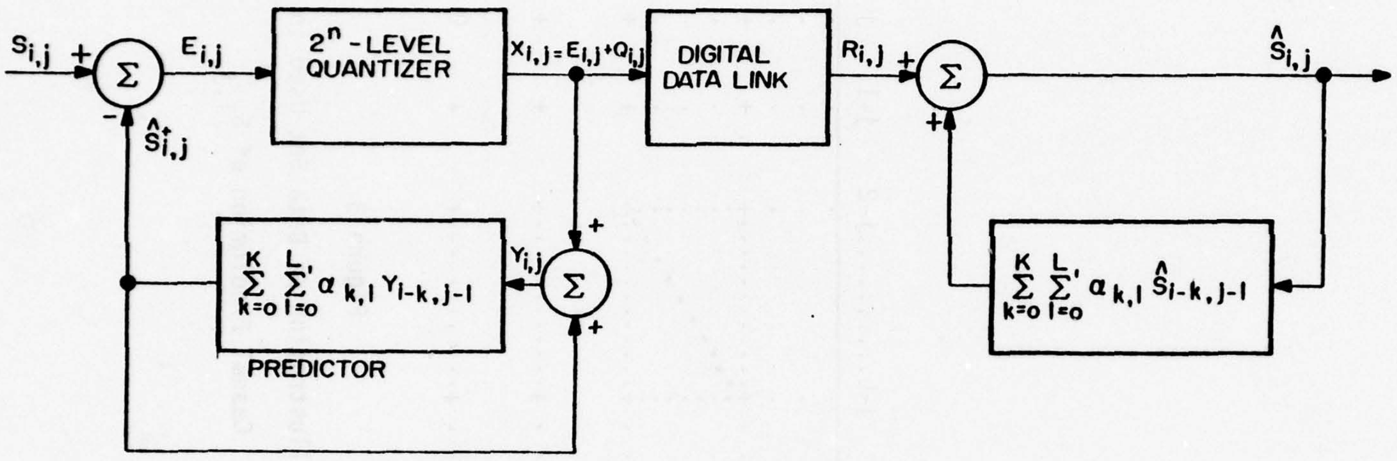

Figure 2

Block Diagram of Two-Dimensional DPCM
Encoding/Decoding System

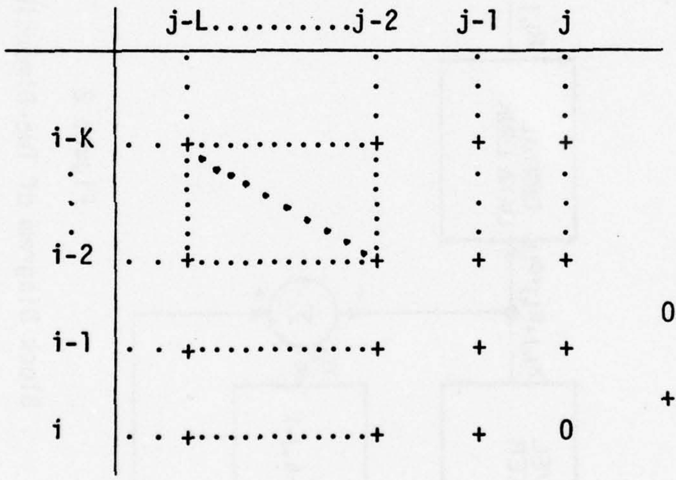

0-element to be predicted

+-elements used in prediction

Figure 3

Illustration of Data Set Used in

Casual Prediction of $S_{i,j}$

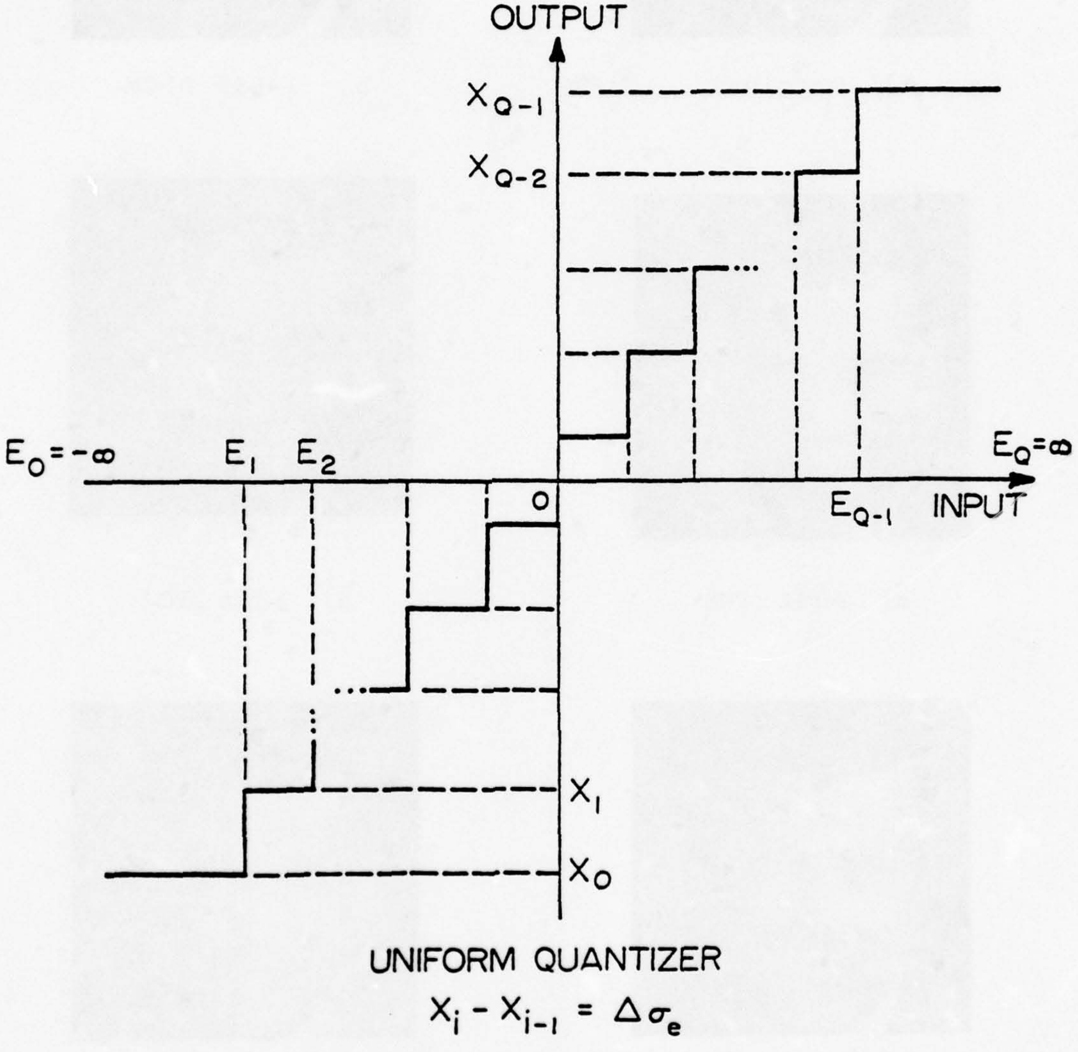

Figure 4

Uniform Quantizer Characteristic

a) Original

b) 1-bit DPCM

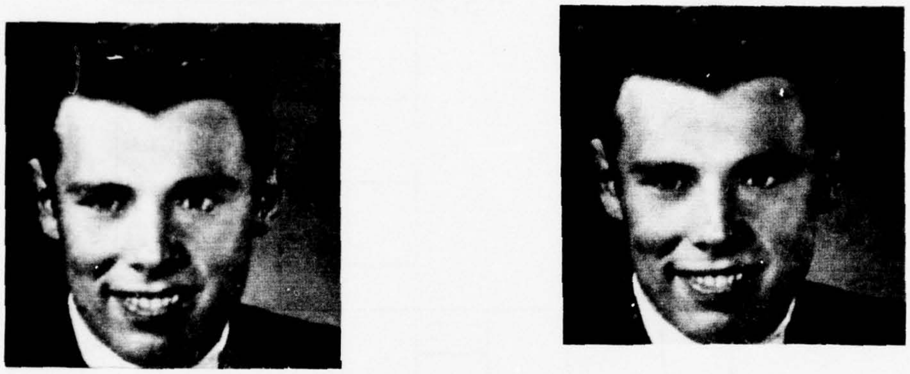

c) 2-bit DPCM

d) 3-bit DPCM

e) 4-bit DPCM

f) 5-bit DPCM

Figure 5

2-D DPCM Encoding of Typical Head-and-Shoulders Image.
Quantization Effects on Reconstructed Image; Gaussian Quantizer.

a) Original

b) 1-bit DPCM

c) 2-bit DPCM

d) 3-bit DPCM

e) 4-bit DPCM

f) 5-bit DPCM

Figure 6

2-D DPCM Encoding of Typical Head-and-Shoulders Image.
Quantization Effects on Reconstructed Image; Laplacian Quantizer.

a) Original b) 1-bit DPCM

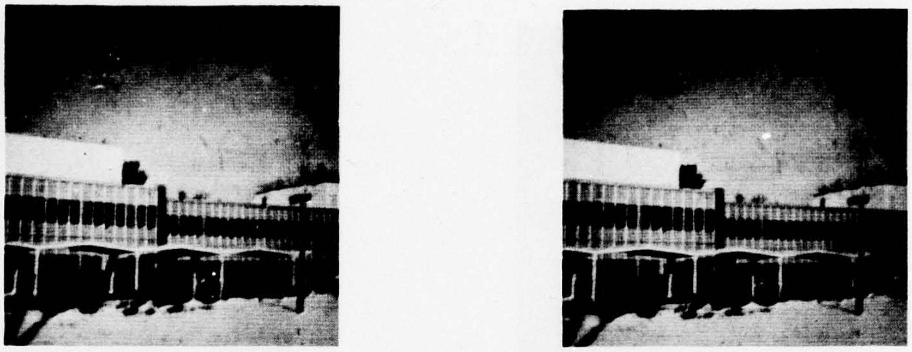

c) 2-bit DPCM d) 3-bit DPCM

e) 4-bit DPCM f) 5-bit DPCM

Figure 7

2-D DPCM Encoding of Typical Outdoor Scene.
Quantization Effects on Reconstructed Image; Gaussian Quantizer.

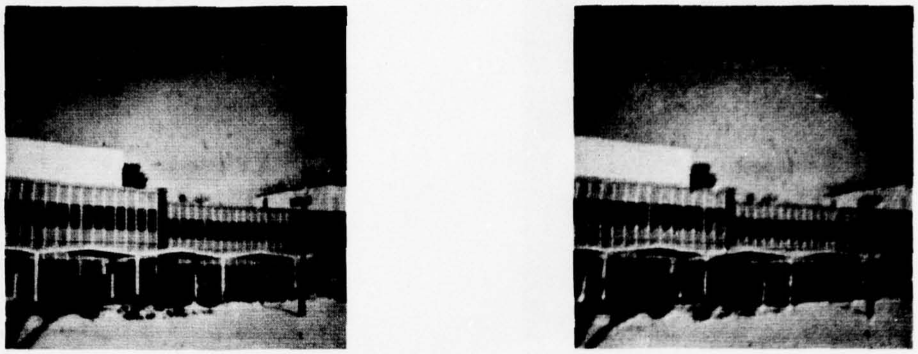

a) Original

b) 1-bit DPCM

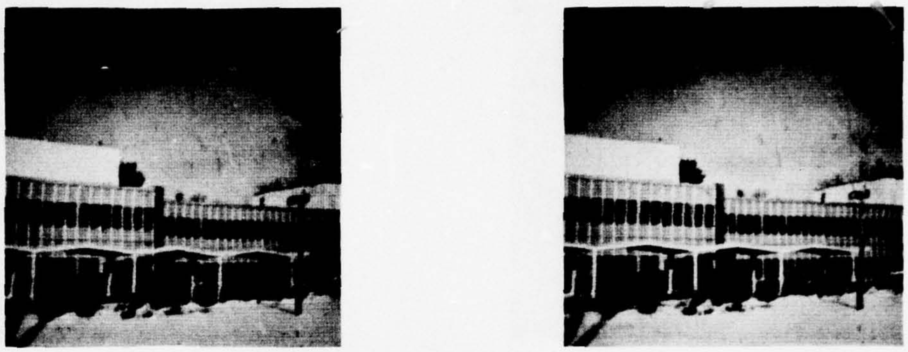

c) 2-bit DPCM

d) 3-bit DPCM

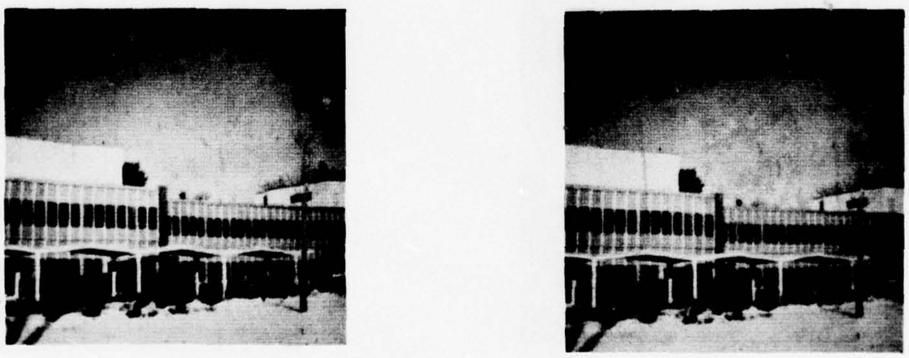

e) 4-bit DPCM

f) 5-bit DPCM

Figure 8

2-D DPCM Encoding of Typical Outdoor Scene.

Quantization Effects on Reconstructed Image; Laplacian Quantizer.

a) Original b) 1-bit DPCM

c) 2-bit DPCM d) 3-bit DPCM

e) 4-bit DPCM f) 5-bit DPCM

Figure 9

Channel Error Effects on 2-D DPCM Image Decoding.

Typical Head-and-Shoulders Image;$P_b=10^{-3}$.

a) Original b) 1-bit DPCM

c) 2-bit DPCM d) 3-bit DPCM

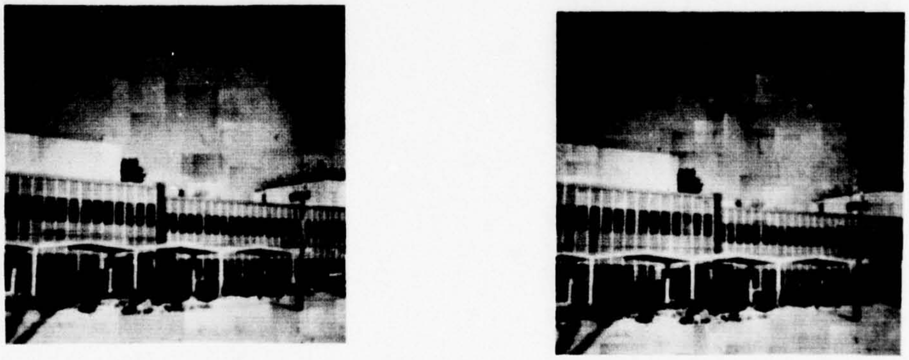

e) 4-bit DPCM f) 5-bit DPCM

Figure 10

Channel Error Effects on 2-D DPCM Image Decoding.

Typical Outdoor Scene; $P_b = 10^{-3}$.

a) Original b) 1-bit DPCM

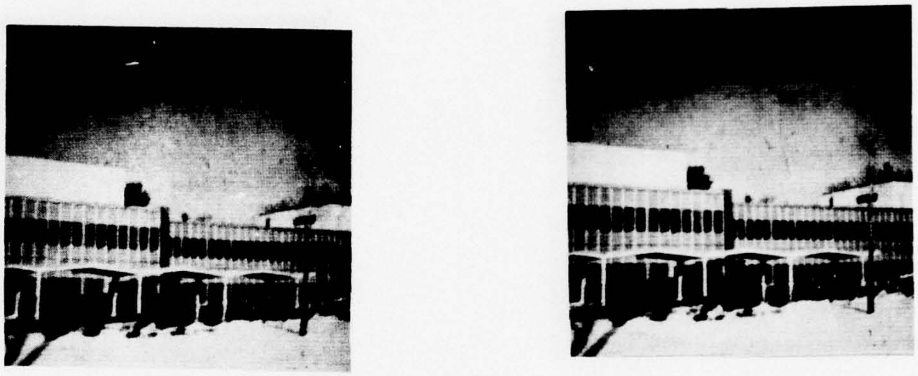

c) 2-bit DPCM d) 3-bit DPCM

e) 4-bit DPCM f) 5-bit DPCM

Figure 11

Channel Error Effects on 2-D DPCM Image Decoding. Typical Outdoor Scene;$P_b=10^{-4}$.

a) Original b) 1-bit DPCM

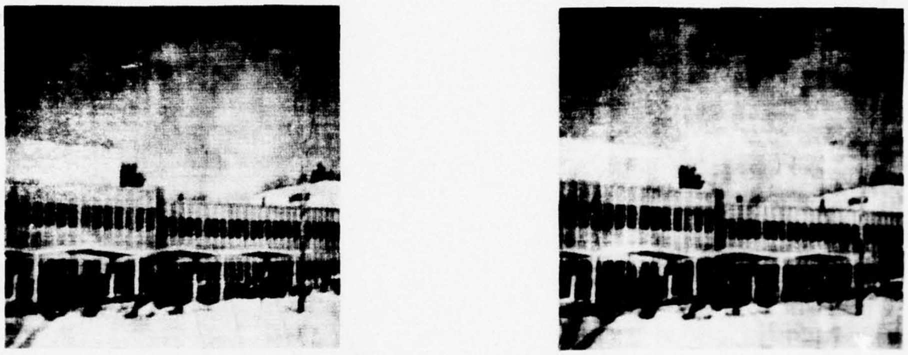

c) 2-bit DPCM d) 3-bit DPCM

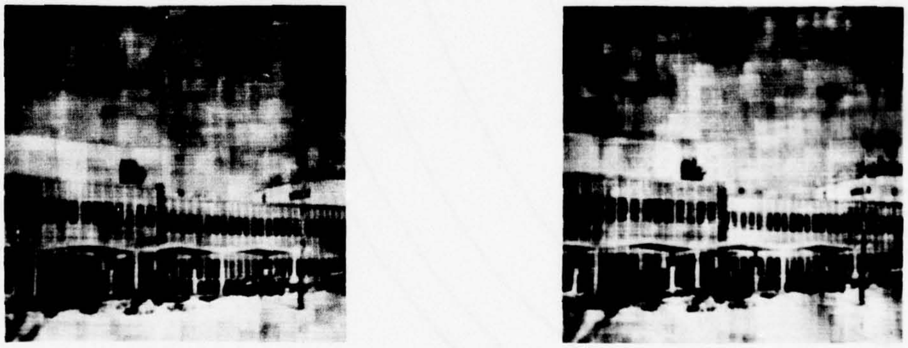

e) 4-bit DPCM f) 5-bit DPCM

Figure 12

Channel Error Effects on 2-D DPCM Image Decoding.

Typical Outdoor Scene; $P_b=5\times10^{-3}$.

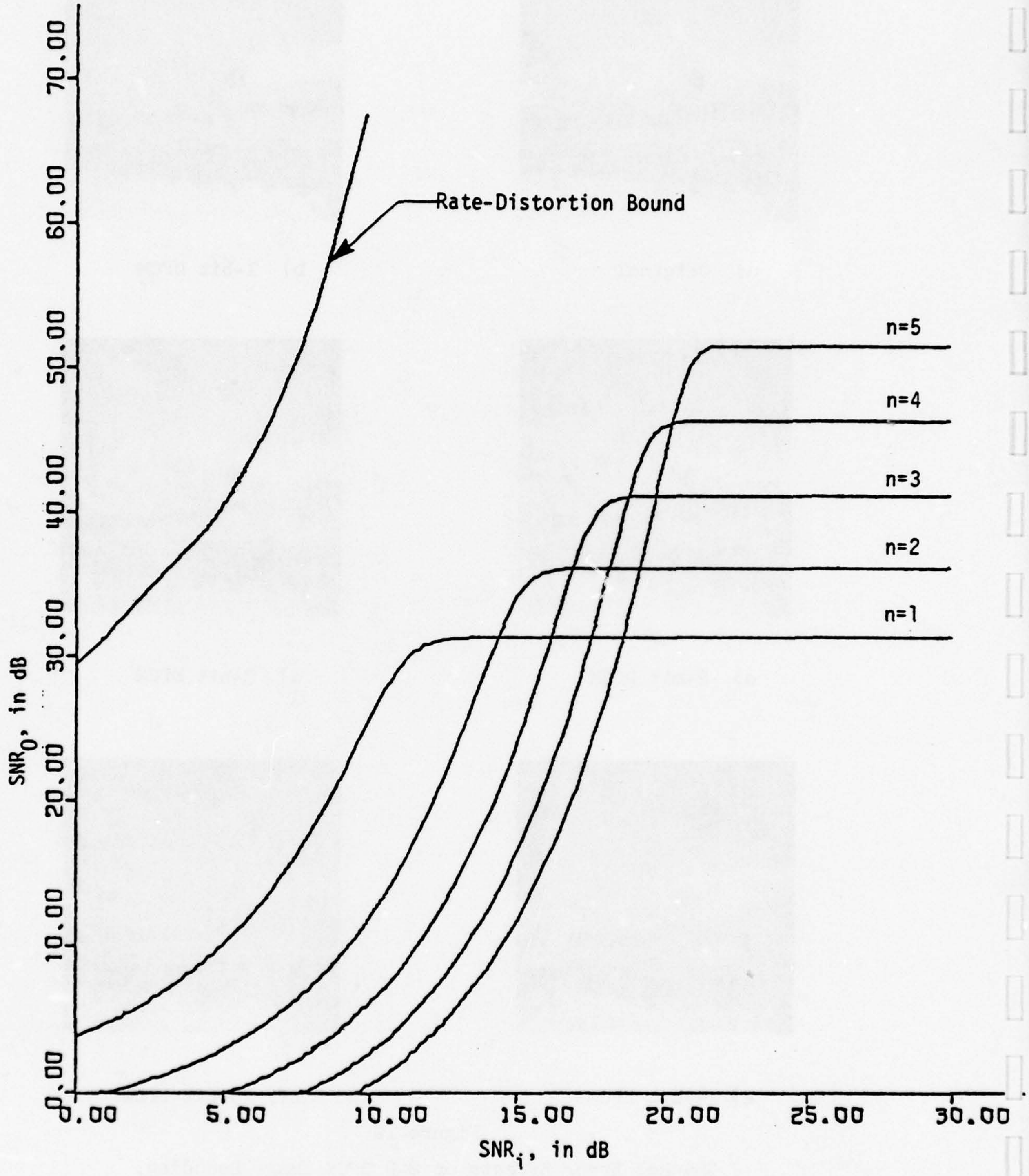

Figure 13

Uncoded 2-D DPCM System Performance for
Head-and-Shoulders Image; Gaussian Quantizer.

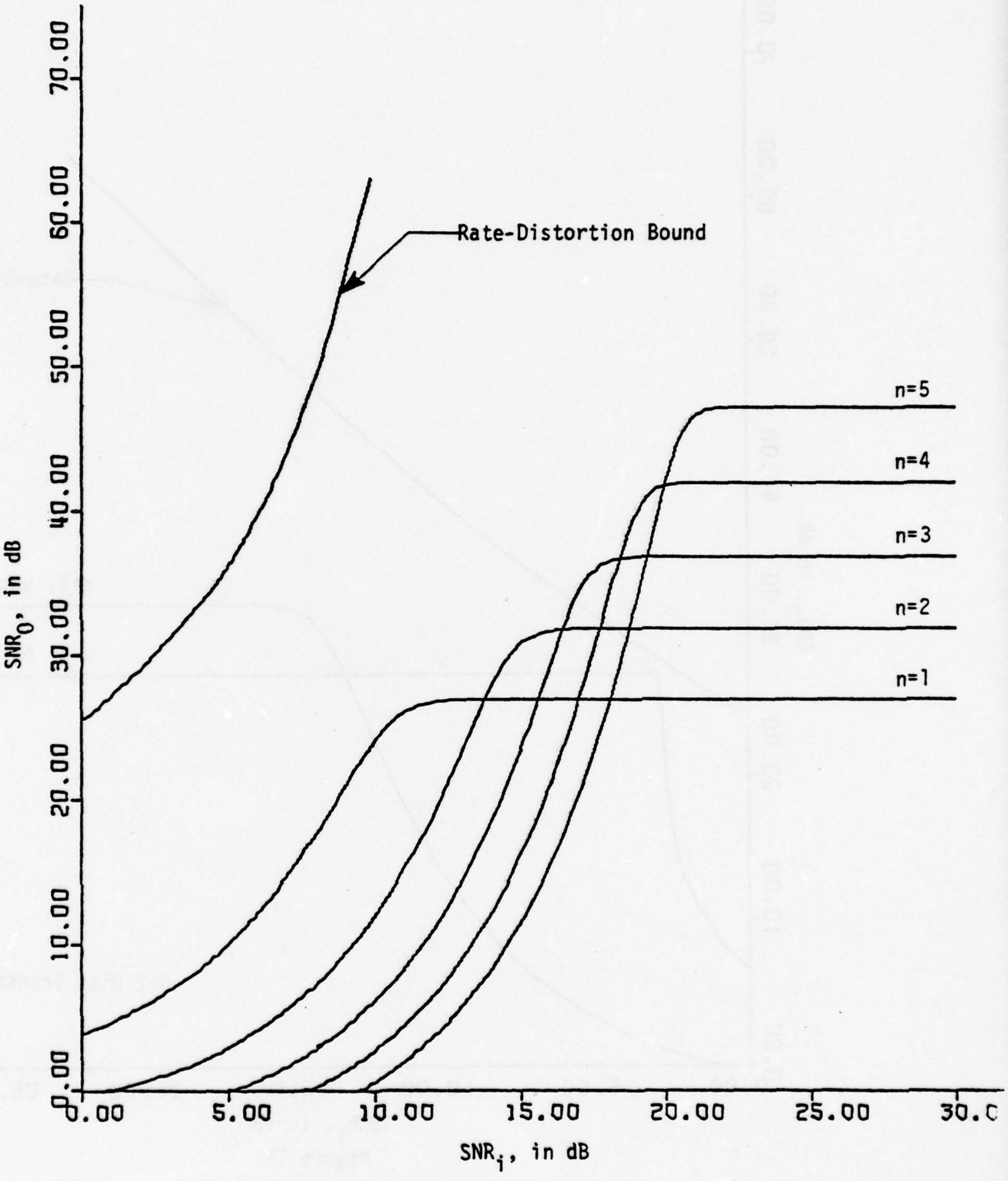

Figure 14

Uncoded 2-D DPCM System Performance for Outdoor Scene; Gaussian Quantizer

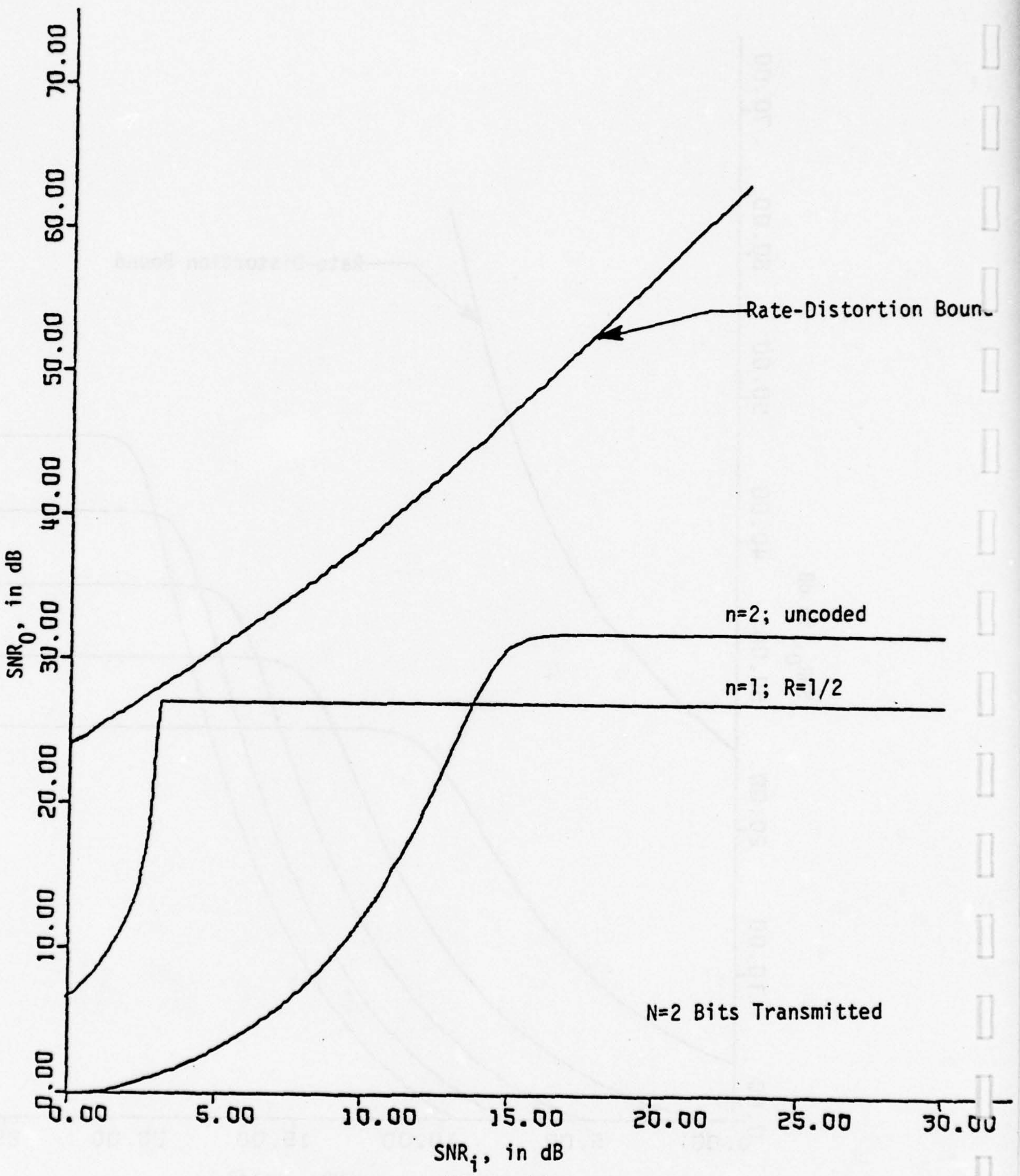

Figure 15

Performance Bounds for Optimum Fixed-Rate Codes;
Outdoor Scene; Gaussian Quantizer.

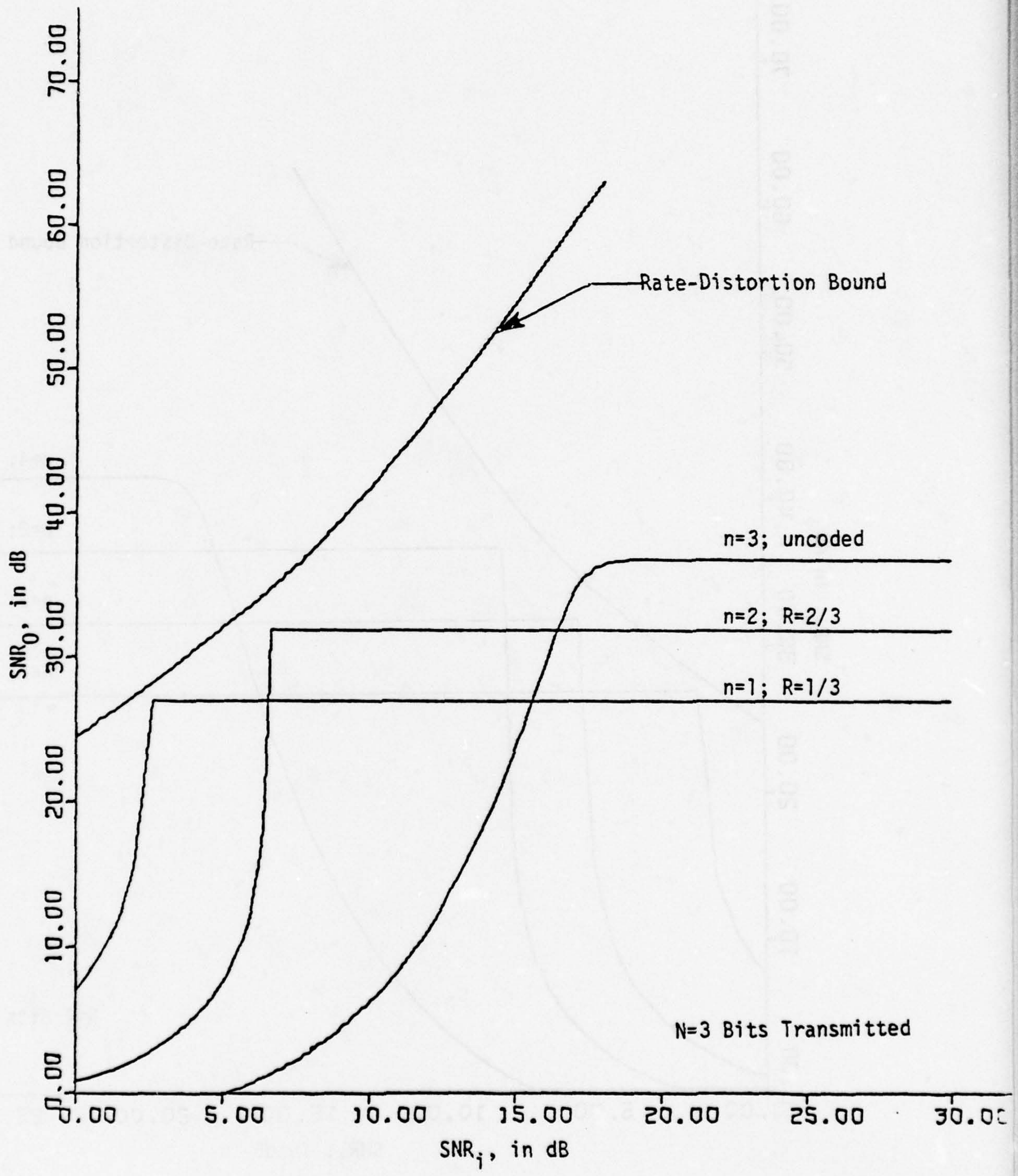

Figure 16

Performance Bounds for Optimum Fixed-Rate Codes;

Outdoor Scene; Gaussian Quantizer.

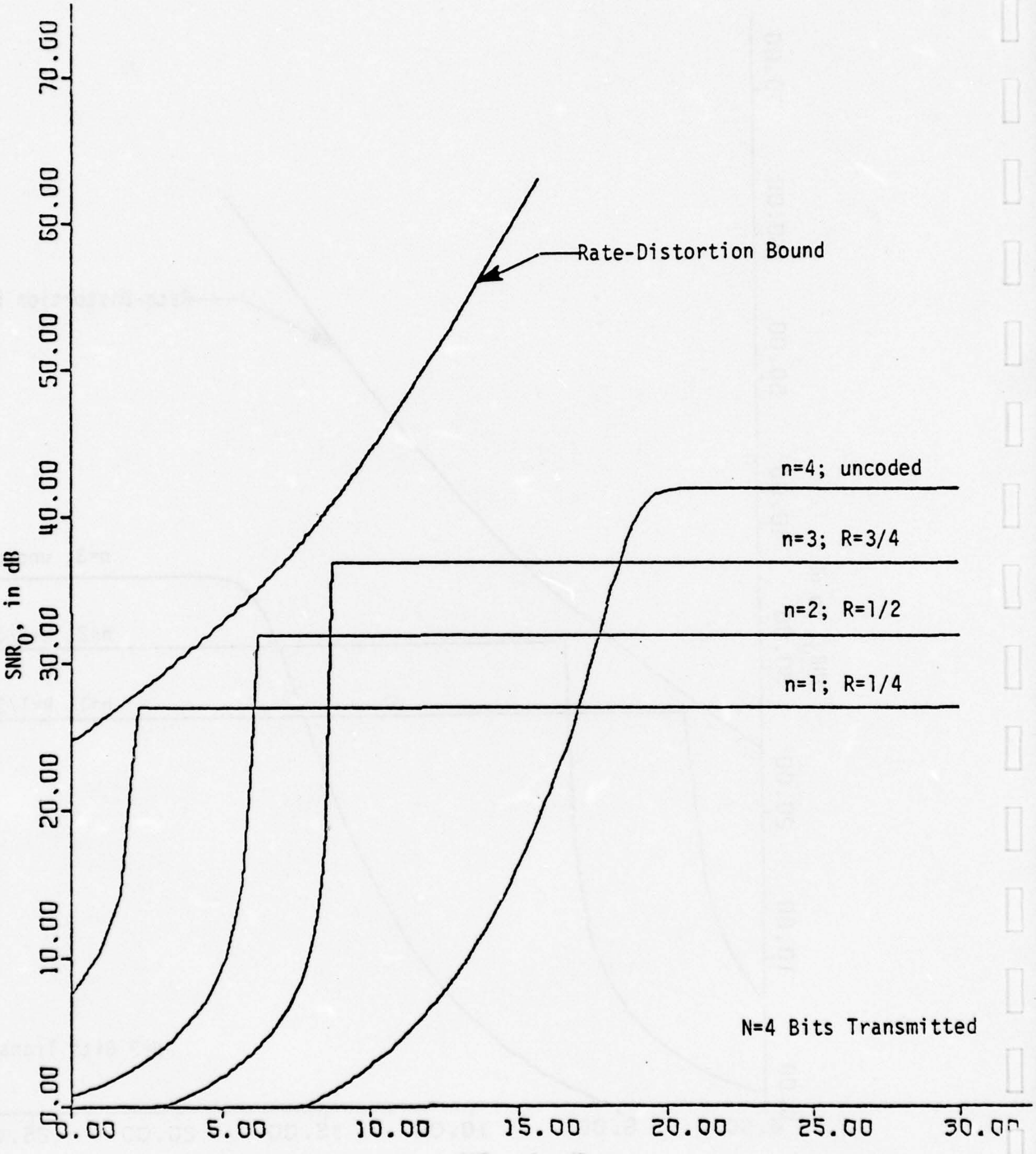

Figure 17

Performance Bounds for Optimum Fixed-Rate Codes;
Outdoor Scene; Gaussian Quantizer.

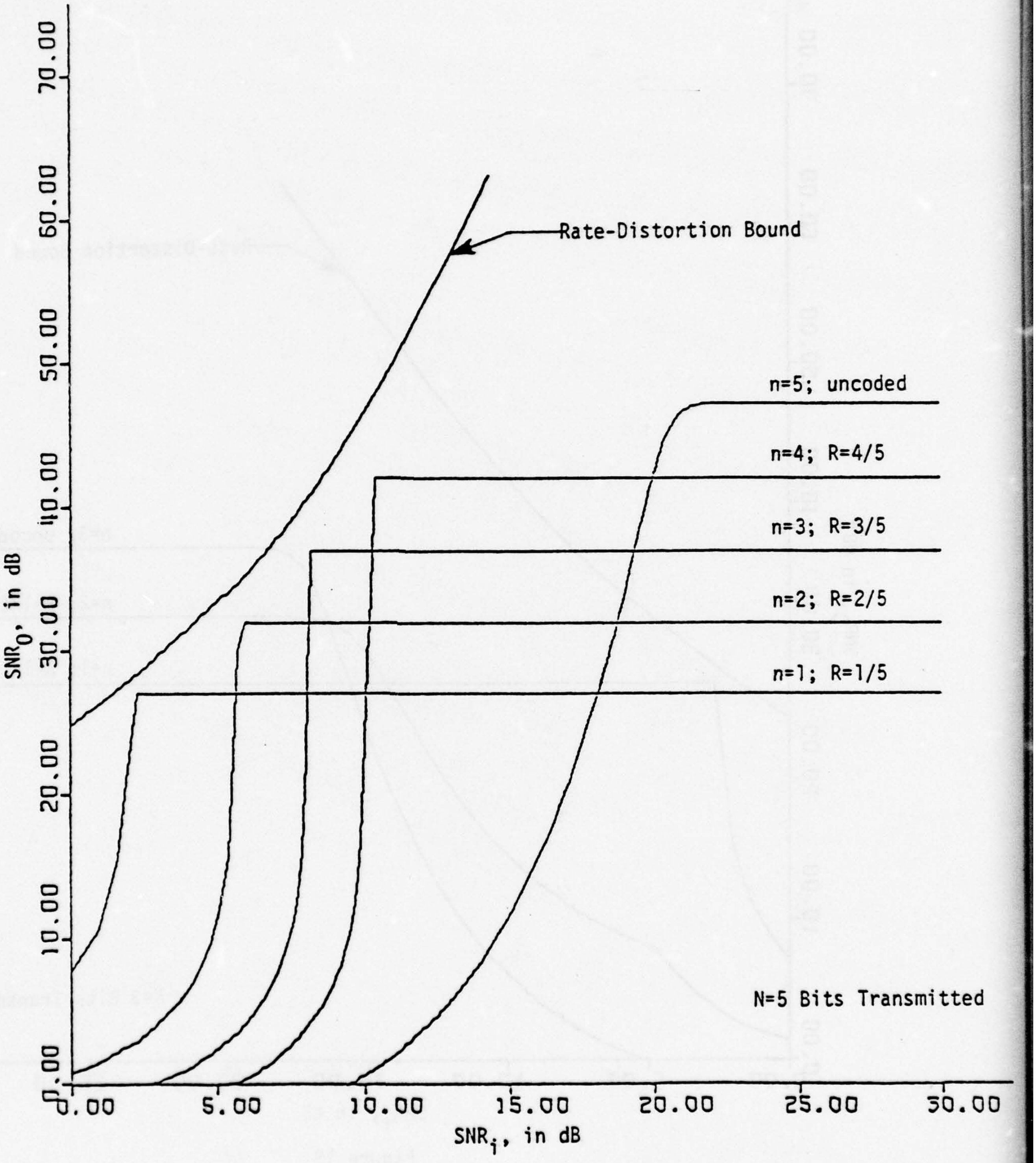

Figure 18

Performance Bounds for Optimum Fixed-Rate Codes; Outdoor Scene; Gaussian Quantizer.

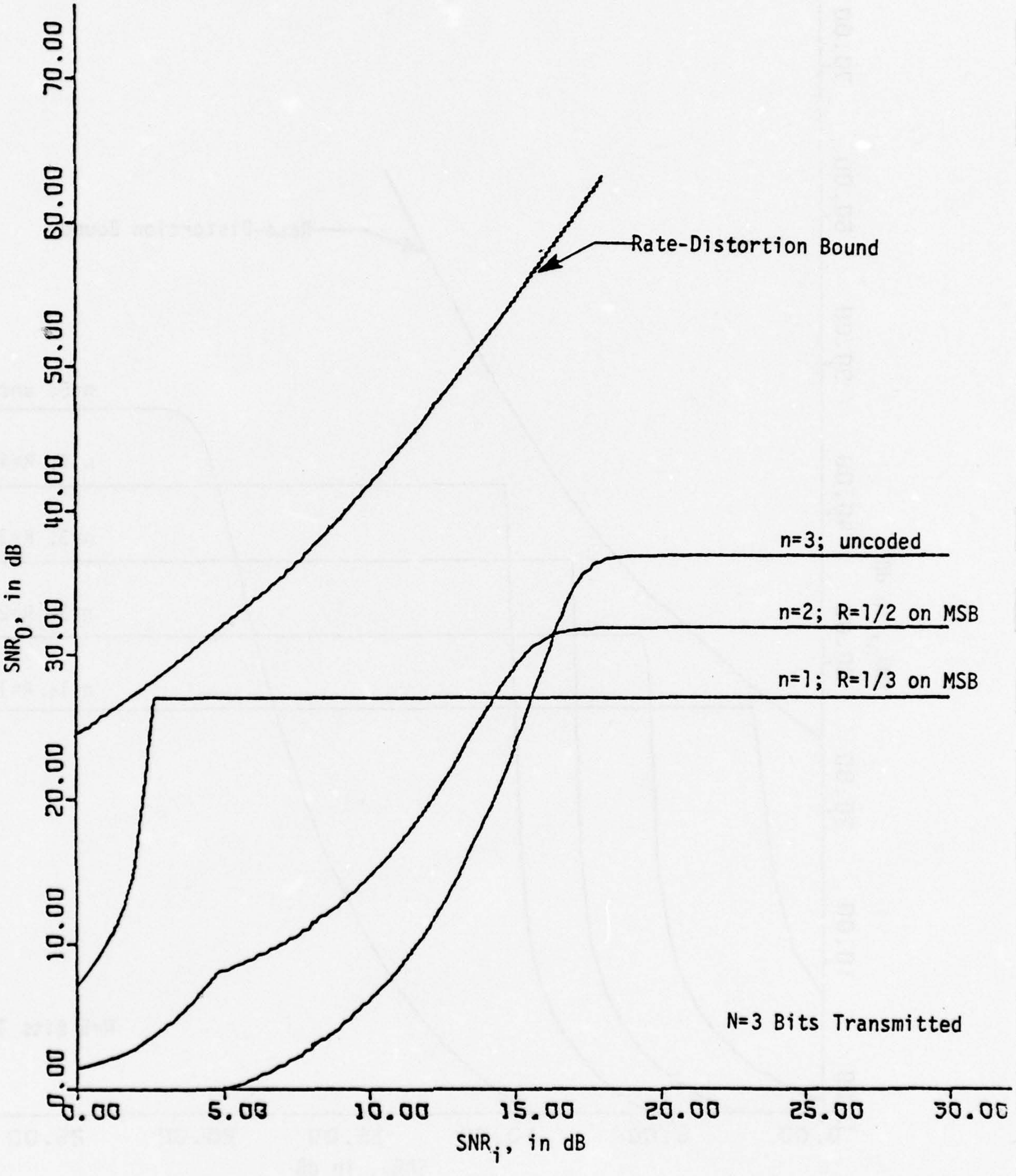

Figure 19

Performance Bounds for Optimum Practical-Rate Codes Combined with No Coding; Outdoor Scene; Gaussian Quantizer.

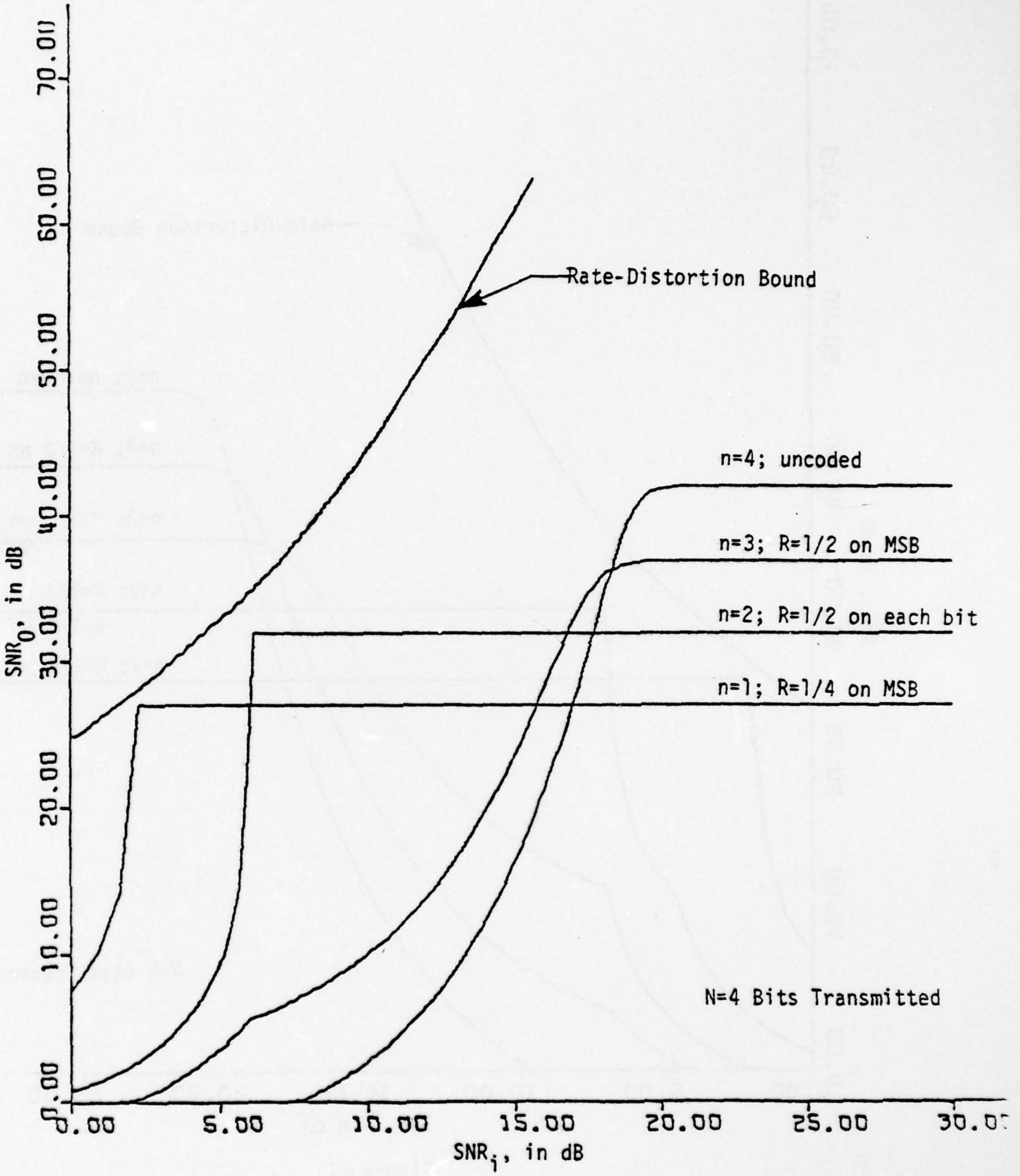

Figure 20

Performance Bounds for Optimum Practical-Rate Codes
Combined with No Coding; Outdoor Scene; Gaussian Quantizer.

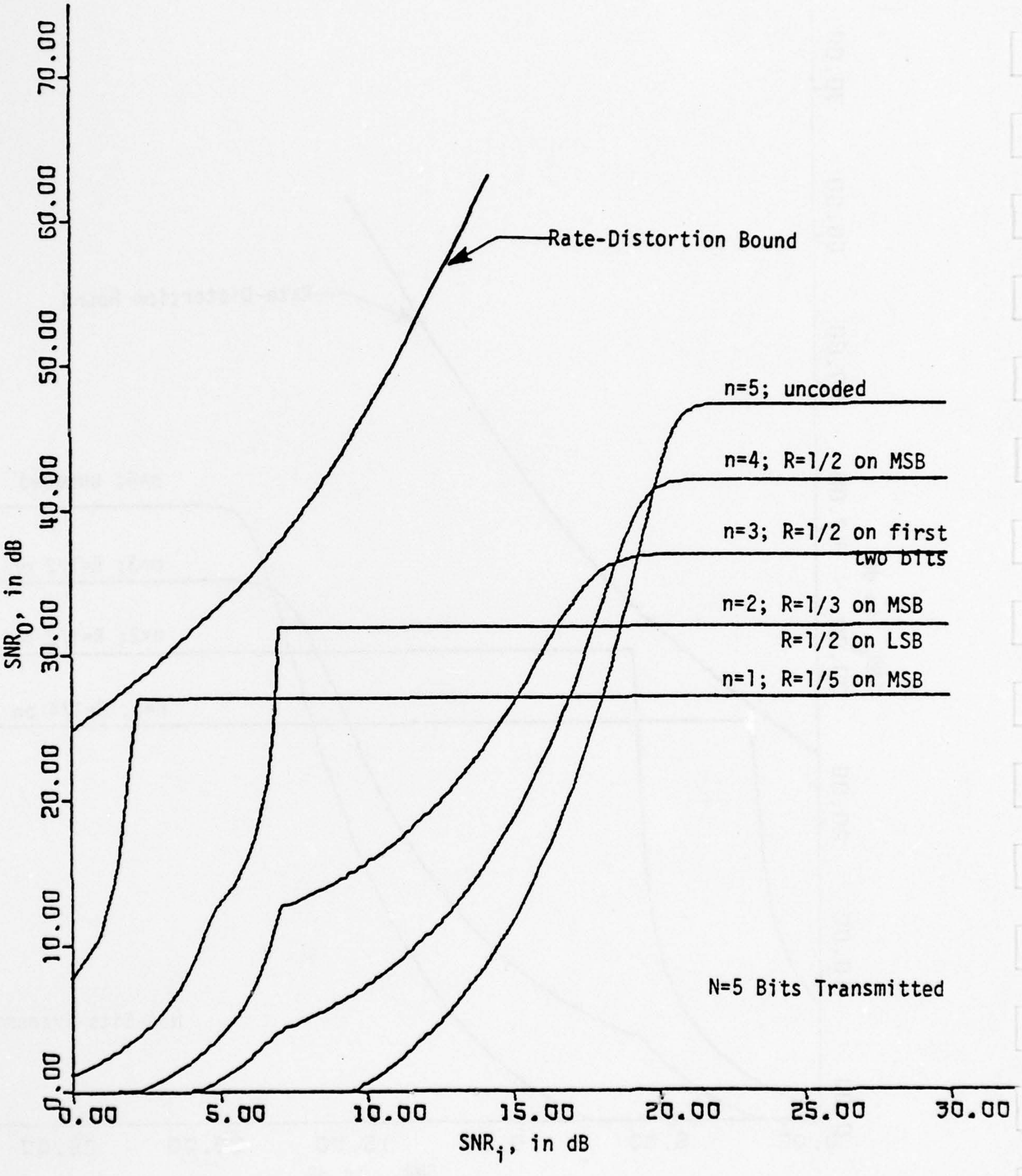

Figure 21

Performance Bounds for Optimum Practical-Rate Codes
Combined with No Coding; Outdoor Scene; Gaussian Quantizer.

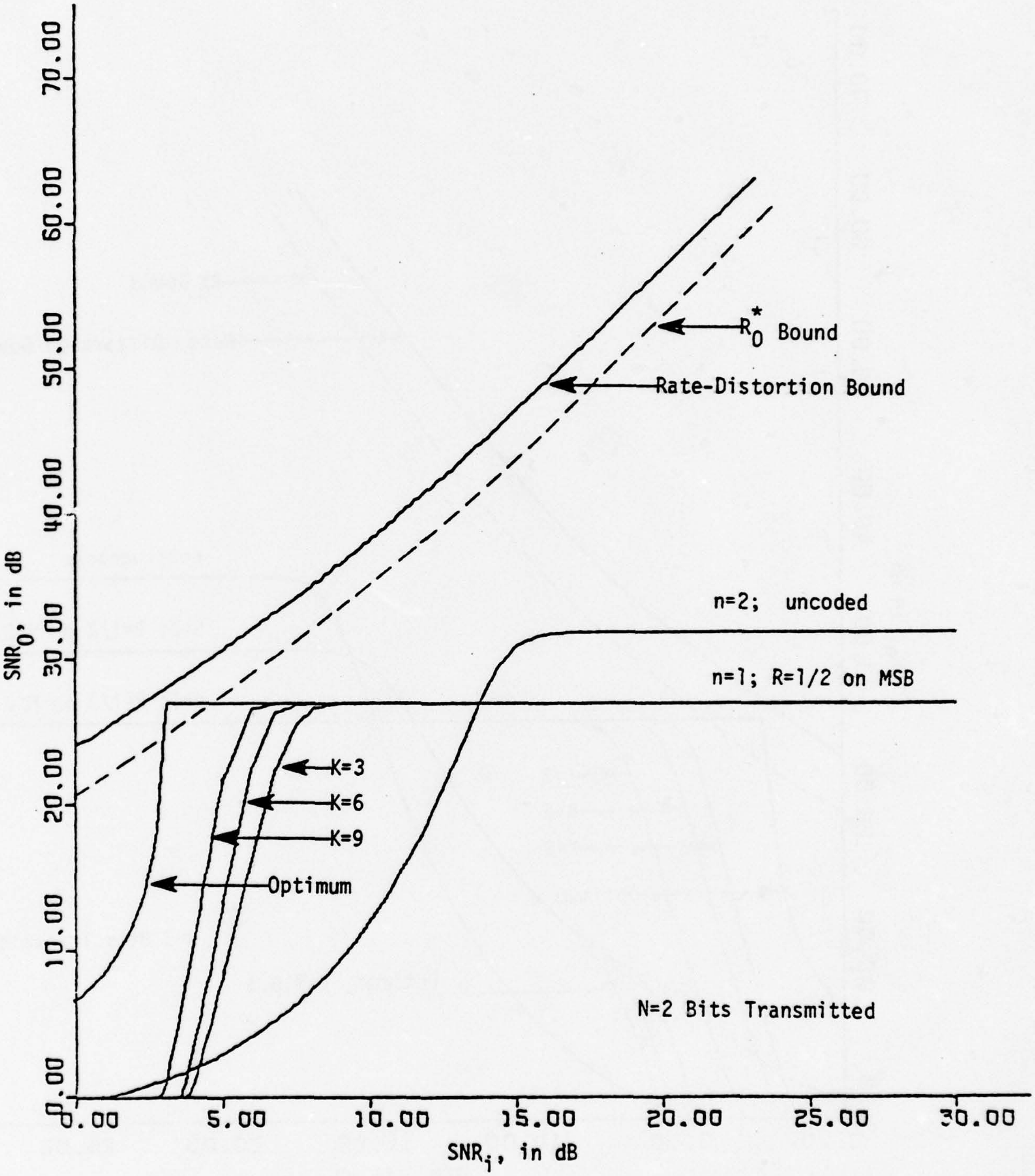

Figure 22

Practical Convolutional Code Performance;
Outdoor Scene; Gaussian Quantizer.

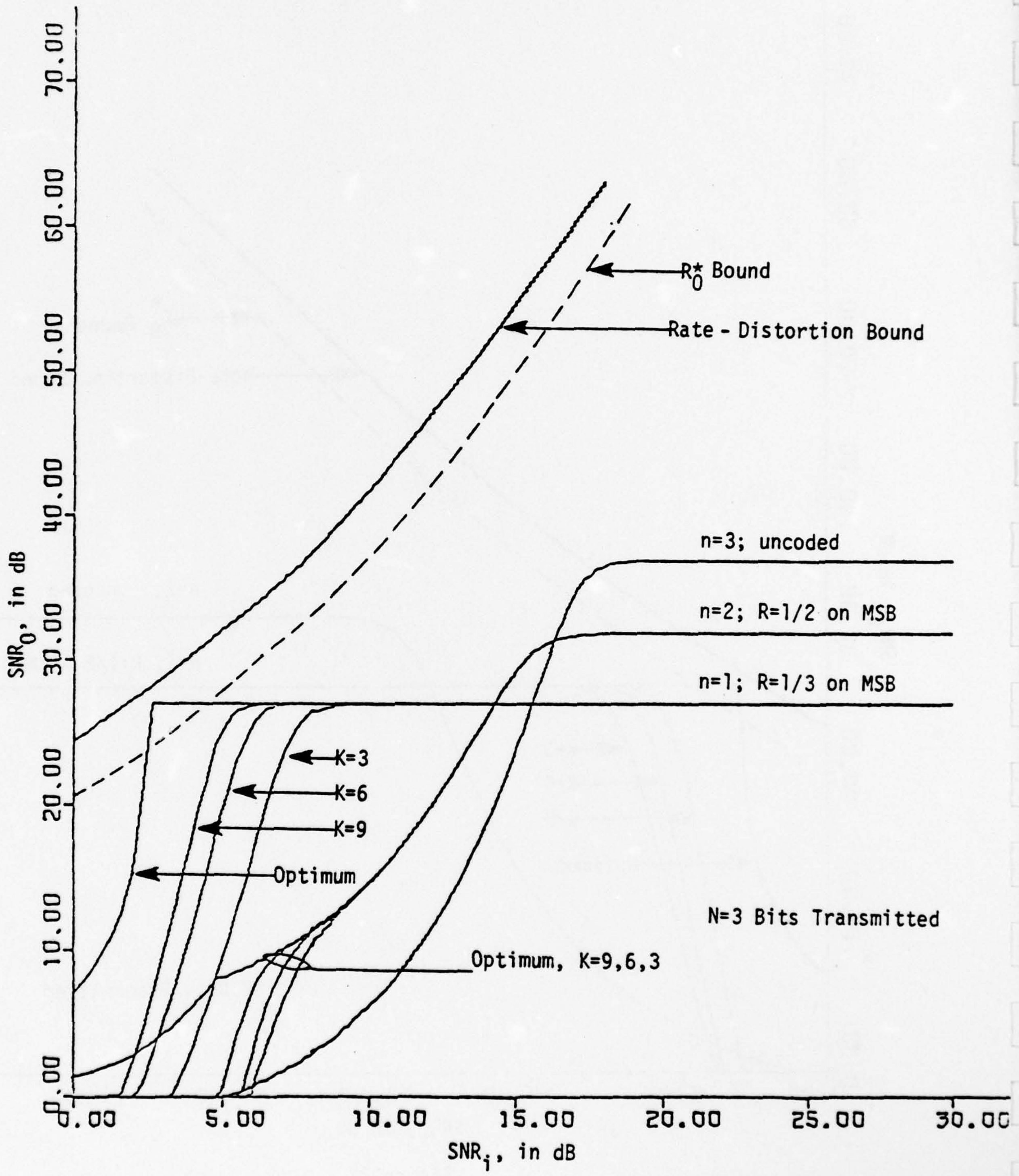

Figure 23

Practical Convolutional Code Performance;
Outdoor Scene; Gaussian Quantizer.

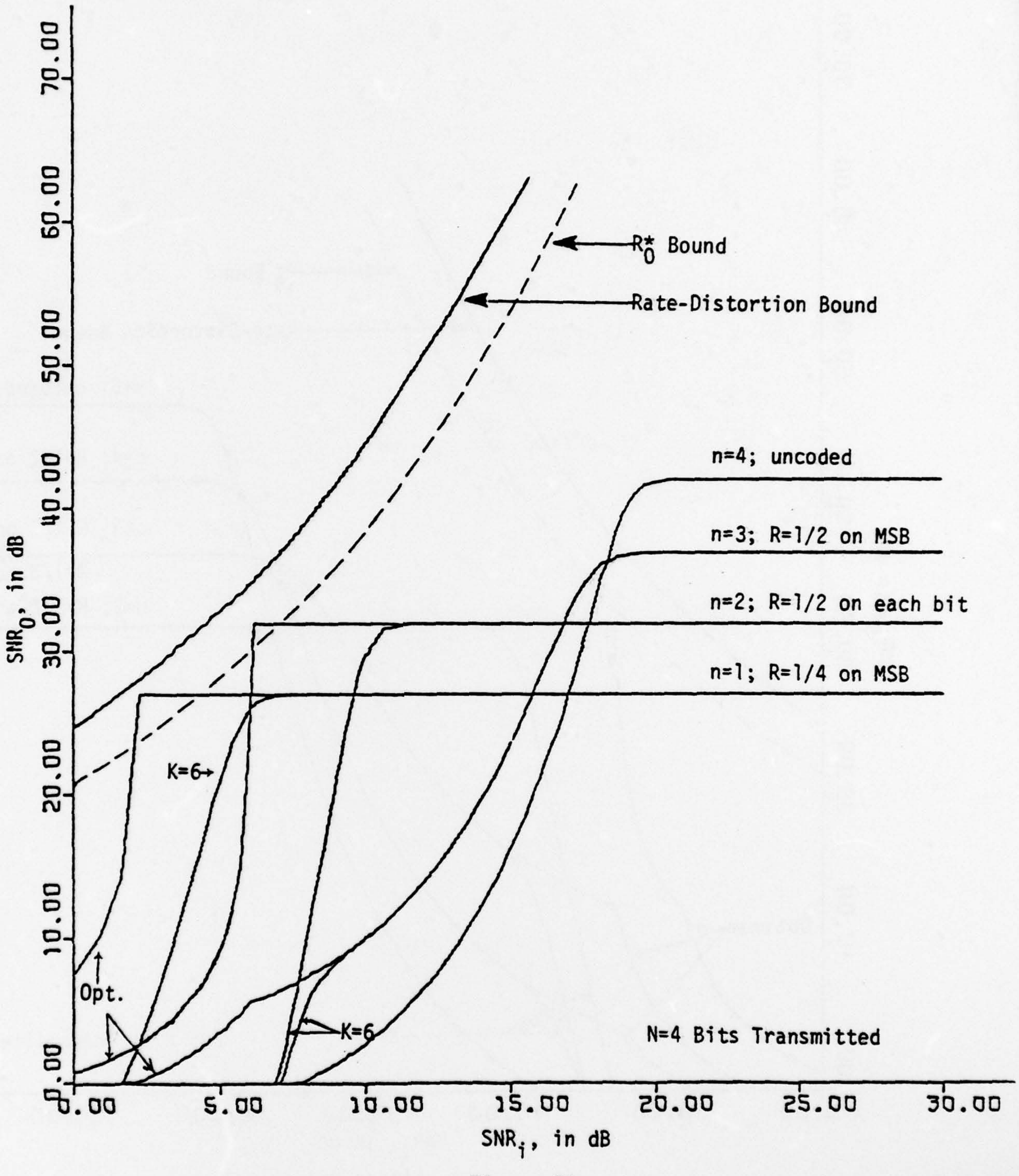

Figure 24

Practical Convolutional Code Performance;
Outdoor Scene; Gaussian Quantizer

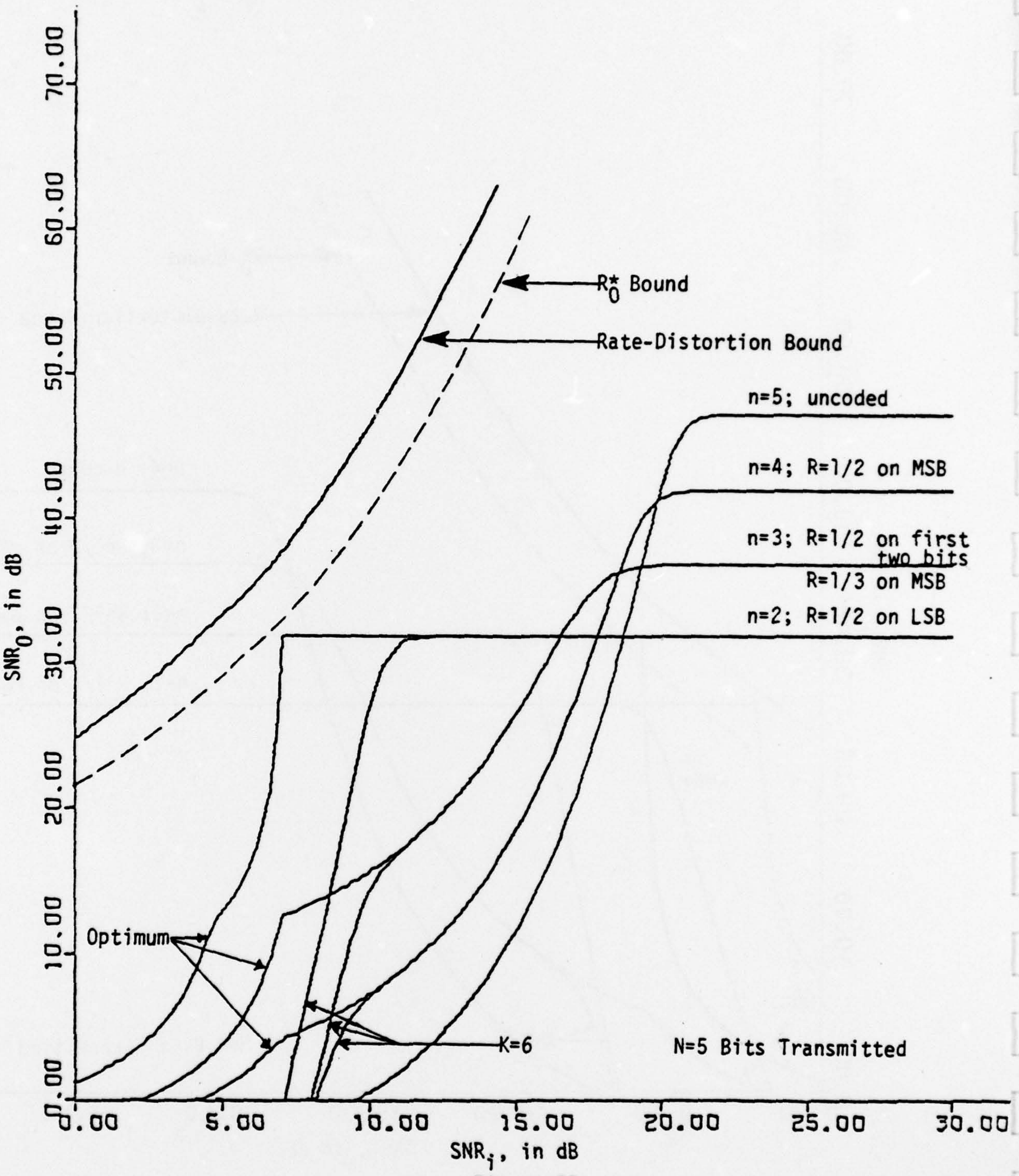

Figure 25

Practical Convolutional Code Performance;
Outdoor Scene; Gaussian Quantizer.

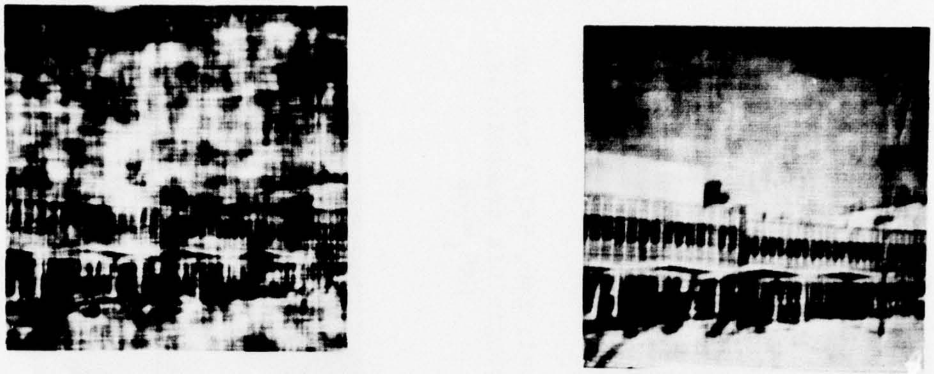

a.) n=2; no coding; $SNR_i$=5dB

b.) n=1; K=6,R=1/2 code on MSB; $SNR_i$=5dB

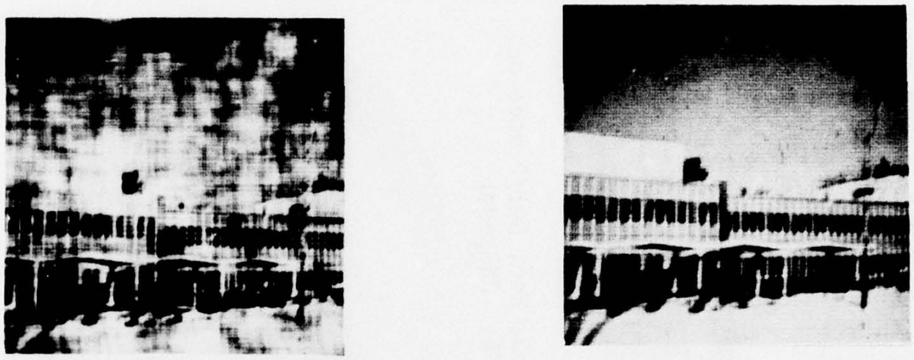

c.) n=2; no coding; $SNR_i$=8dB

d.) n=1; K=6, R=1/2 code on MSB; $SNR_i$=8dB

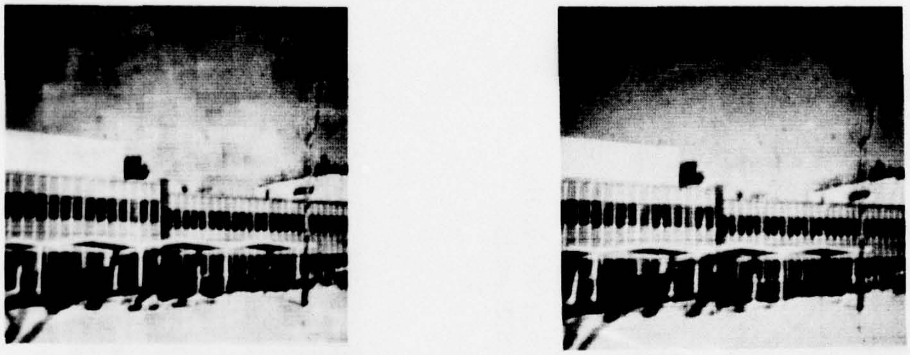

e.) n=2; no coding; $SNR_i$=12dB

f.) n=1; K=6, R=1/2 code on MSB; $SNR_i$=12dB

Figure 26

Simulation Results on Outdoor Scene; N=2 Bits Transmitted.

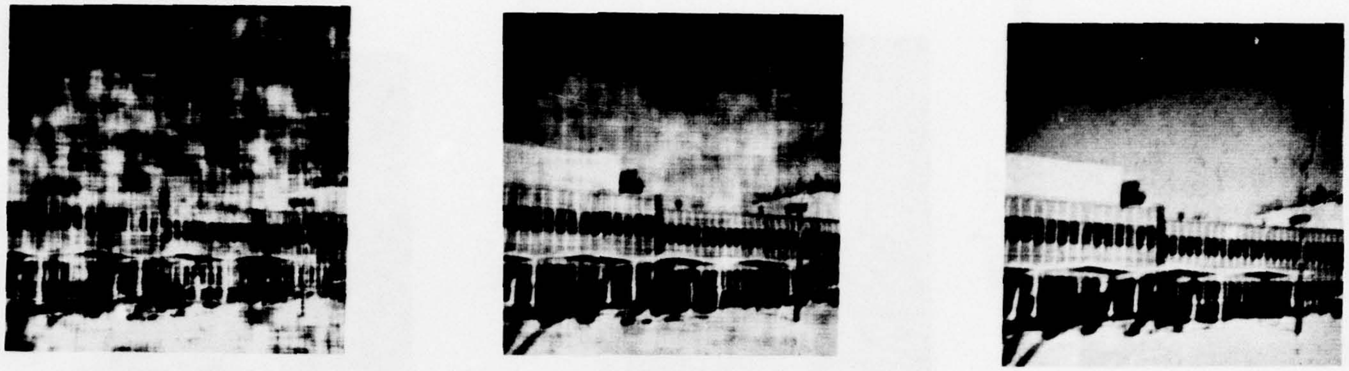

a.) n=3; no coding; $SNR_i$=9dB

b.) n=2; K=6, R=1/2 code on MSB; $SNR_i$=9dB

c.) n=1; K=6, R=1/3 code on single bit transmitted; $SNR_i$=9dB

d.) n=3; no coding; $SNR_i$=15dB

e.) n=2; K=6, R=1/2 code on MSB; $SNR_i$=15dB

f.) n=1; K=6, R=1/3 code on single bit transmitted; $SNR_i$=15dB

Figure 27

Simulation Results on Outdoor Scene; N=3 Bits Transmitted.

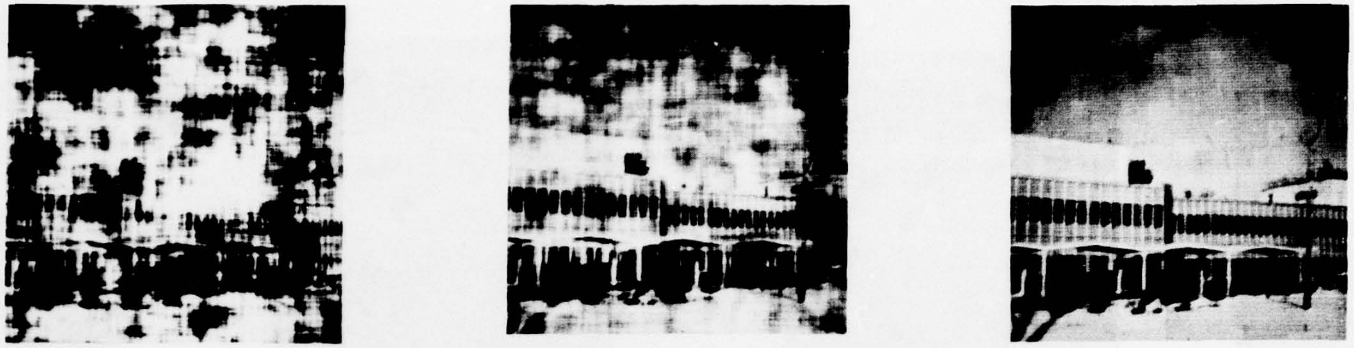

a.) n=4; no coding; $SNR_i$=9dB

b.) n=3; K=6, R=1/2 code on MSB; $SNR_i$=9dB

c.) n=2; K=6, R=1/2 code on each bit transmitted; $SNR_i$=9dB

d.) n=4; no coding; $SNR_i$=16dB

e.) n=3; K=6, R=1/2 code on MSB; $SNR_i$=16dB

f.) n=2; K=6, R=1/2 code on each bit transmitted; $SNR_i$=16dB

Figure 28

Simulation Results on Outdoor Scene; N=4 Bits Transmitted.

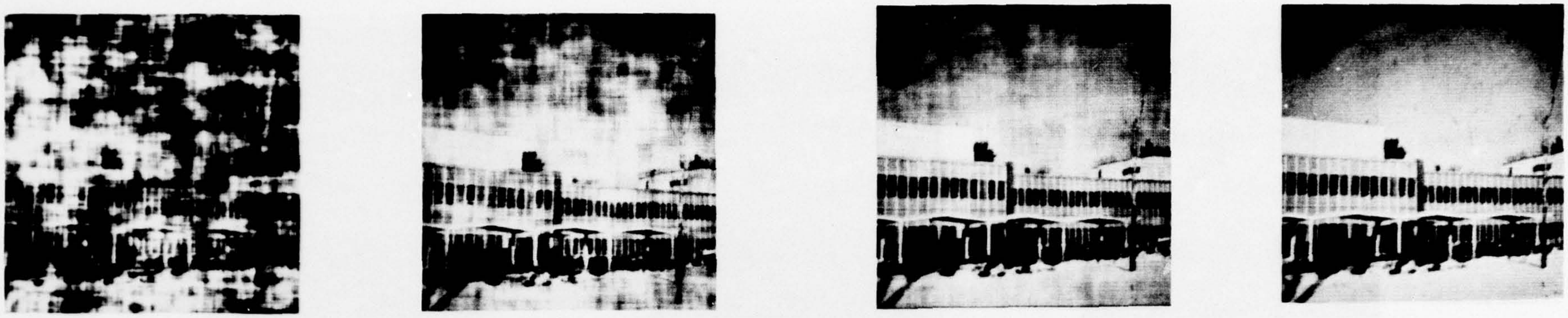

a.) n=5; no coding; $SNR_i$=12dB

b.) n=4; K=6, R=1/2 code on MSB ; $SNR_i$=12dB

c.) n=3; K=6, R=1/2 code on two MSB's; $SNR_i$=12dB

d.) n=2; K=6,R=1/3 cod on MSB, R=1/2 code on LSB; $SNR_i$=12dB

e.) n=5; no coding; $SNR_i$=18dB

f.) n=4; K=6, R=1/2 code on MSB; $SNR_i$=18dB

g.) n=3; K=6, R=1/2 code on two MSB's; $SNR_i$=18dB

h.) n=2; K=6, R=1/3 co on MSB, R=1/2 code on LSB; $SNR_i$=18dB

Figure 29

Simulation Results on Outdoor Scene; N=5 Bits Transmitted.

a.) n=3; no coding; $SNR_i$=9dB

b.) n=2; K=6, R=1/2 code on MSB ; $SNR_i$=9dB

c.) n=1; K=6, R=1/3 code on single bit transmitted; $SNR_i$=9dB

d.) n=3; no coding; $SNR_i$=15dB

e.) n=2; K=6, R=1/2 code on MSB; $SNR_i$=15dB

f.) n=1; K=6, R=1/3 code on single bit transmitted; $SNR_i$=15dB

Figure 30

Simulation Results on Head-and-Shoulders Image; N=3 Bits Transmitted.

# DISTRIBUTION LIST FOR ONR ELECTRONIC AND SOLID STATE SCIENCES

| | |
|---|---|
| Director<br>Advanced Research Projects Agency<br>Attn: Technical Library<br>1400 Wilson Boulevard<br>Arlington, Virginia 22209 | 1 copy |
| Office of Naval Research<br>Electronics Program Office (Code 427)<br>800 North Quincy Street<br>Arlington, Virginia 22217 | 1 copy |
| Office of Naval Research<br>Code 105<br>800 North Quincy Street<br>Arlington, Virginia 22217 | 6 copies |
| Director<br>Naval Research Laboratory<br>455 Overlook Avenue, S.W.<br>Washington, D. C. 20375<br>Attn: Technical Library | 6 copies |
| Code 5200 | 1 copy |
| 5210 | 1 copy |
| 5270 | 1 copy |
| 6400 | 1 copy |
| Office of the Director of Defense<br>Research and Engineering<br>Information Office Library Branch<br>The Pentagon<br>Washington, D. C. 20301 | 1 copy |
| Defense Documentation Center<br>Cameron Station<br>Alexandria, Virginia 22314 | 12 copies |
| Commanding Officer<br>Office of Naval Research Branch Office<br>536 South Clark Street<br>Chicago, Illinois 60605 | 1 copy |
| San Francisco Area Office<br>Office of Naval Research<br>50 Fell Street<br>San Francisco, California 94102 | 1 copy |

Commanding Officer 1 copy
Office of Naval Research Branch Office
1030 East Green Street
Pasadena, California 91101

Commanding Officer 1 copy
Office of Naval Research Branch Office
495 Summer Street
Boston, Massachusetts 02210

New York Area Office 1 copy
Office of Naval Research
715 Broadway, 5th Floor
New York, New York 10003

ODDR&E Advisory Group on Electron Devices 1 copy
201 Varick Street
New York, New York 10014

Naval Air Development Center 1 copy
Attn: Technical Library
Johnsville
Warminster, Pennsylvania 18974

Naval Weapons Center
China Lake, California 93555
Attn: Technical Library 1 copy
Code 6010 1 copy

Naval Research Laboratory 1 copy
Underwater Sound Reference Division
Technical Library
P. O. Box 8337
Orlando, Florida 32806

Navy Underwater Sound Laboratory 1 copy
Technical Library
Fort Trumbull
New London, Connecticut 06320

Commandant, Marine Corps 1 copy
Scientific Advisor (Code AX)
Washington, D. C. 20380

Naval Ordinance Station 1 copy
Technical Library
Indian Head, Maryland 20640

Naval Postgraduate School
Monterey, California 93940
Attn: Technical Library 1 copy
Electrical Engineering Department 1 copy

Naval Missile Center 1 copy
Technical Library (Code 5632.2)
Point Mugu, California 93010

Naval Electronics Laboratory Center
San Diego, California
Attn: Technical Library 1 copy
Code 2300 1 copy
2600 1 copy
4800 1 copy

Naval Undersea Warfare Center 1 copy
Technical Library
3202 East Foothill Boulevard
Pasadena, California 91107

Naval Weapons Laboratory 1 copy
Technical Library
Dahlgren, Virginia 22448

Naval Ship Research and Development Center 1 copy
Central Library Code L42 and L43)
Washington, D. C. 20007

Naval Surface Weapons Center
White Oak Laboratory
Silver Spring, Maryland 20910
Attn: Technical Library 1 copy
Code 200 1 copy
212 1 copy

Deputy Chief of Naval Operations (Development) 1 copy
Technical Analysis and Advisory Group (Code NOP-077D)
Washington, D. C. 20350

Commander
Naval Air Systems Command
Washington, D. C.
Attn: Code 310 1 copy
360 1 copy

Commander
Naval Electronics Systems Command
Washington, D. C. 20360
Attn: Code 304 1 copy
310 1 copy

Commander 1 copy
Naval Sea Systems Command
Washington, D. C. 20360

Naval Surface Weapons Center 1 copy
Attn: Library
Dahlgren, Virginia 22448

Air Force Office of Scientific Research 1 copy
Attn: Electronic and Solid State Sciences Division
Department of the Air Force
Washington, D. C. 20333

Air Force Weapon Laboratory 1 copy
Technical Library
Kirtland Air Force Base
Albuquerque, New Mexico 87117

Air Force Avionics Laboratory 1 copy
Air Force Systems Command
Technical Library
Wright-Patterson Air Force Base
Dayton, Ohio 45433

Air Force Cambridge Research Laboratory 1 copy
L. G. Hanscom Field
Technical Library
Cambridge, Massachusetts 02138

Harry Diamond Laboratories 1 copy
Technical Library
Connecticut Avenue at Van Ness, N. W.
Washington, D. C. 20438

U. S. Army Research Office 1 copy
Box CM, Duke Station
Durham, North Carolina 27706

Director 1 copy
U. S. Army Engineering Research
and Development Laboratories
Fort Belvoir, Virginia 22060
Attn: Technical Documents Center

Director National Bureau of Standards 1 copy
Attn: Technical Library
Washington, D. C. 20234

Superintendent 1 copy
Materials Sciences Division
Naval Research Laboratory
4555 Overlook Avenue S.W.
Washington, D.C. 20375

SUPPLEMENTAL LIST FOR SYSTEMS AREA

Office of Naval Research 2 copies
800 N. Quincy Street
Arlington, Virginia 22217
Attn: Code 430

Naval Research Laboratory 1 copy
4555 Overlook Avenue, S. W.
Washington, D. C. 20375
Attn: Code 5400

Naval Electronics Laboratory Center
San Diego, California 92152
Attn: Code 3000 1 copy
5000 1 copy
5600 1 copy

Air Force Office of Scientific Research 1 copy
Mathematical and Information Sciences Directorate
1400 Wilson Blvd.
Washington, D. C. 20333

## REPORT DOCUMENTATION PAGE

READ INSTRUCTIONS BEFORE COMPLETING FORM

| | | |
|---|---|---|
| 1. REPORT NUMBER<br>TR 78-1 | 2. GOVT ACCESSION NO. | 3. RECIPIENT'S CATALOG NUMBER |
| 4. TITLE (and Subtitle)<br>COMBINED SOURCE-CHANNEL CODING OF IMAGE | | 5. TYPE OF REPORT & PERIOD COVERED<br>Technical Report |
| | | 6. PERFORMING ORG. REPORT NUMBER |
| 7. AUTHOR(s)<br>J. W. Modestino and D. G. Daut | | 8. CONTRACT OR GRANT NUMBER(s)<br>N00014-75-C-0281 |
| 9. PERFORMING ORGANIZATION NAME AND ADDRESS<br>Electrical & Systems Engineering Dept.<br>School of Engineering<br>Rensselaer Polytechnic Institute, Troy, N.Y.12181 | | 10. PROGRAM ELEMENT, PROJECT, TASK AREA & WORK UNIT NUMBERS<br>NR 375-971 |
| 11. CONTROLLING OFFICE NAME AND ADDRESS<br>Dept. of the Navy, Office of Naval Research,<br>Electronic & Solid State Sciences Program<br>Arlington, VA 22217 | | 12. REPORT DATE<br>September 1978 |
| | | 13. NUMBER OF PAGES<br>61 |
| 14. MONITORING AGENCY NAME & ADDRESS(if different from Controlling Office) | | 15. SECURITY CLASS. (of this report) |
| | | 15a. DECLASSIFICATION/DOWNGRADING SCHEDULE |

16. DISTRIBUTION STATEMENT (of this Report)

Distribution unlimited; approved for public release

17. DISTRIBUTION STATEMENT (of the abstract entered in Block 20, if different from Report)

18. SUPPLEMENTARY NOTES

19. KEY WORDS (Continue on reverse side if necessary and identify by block number)

Image Processing, Image Coding, DPCM Coding of Images

20. ABSTRACT (Continue on reverse side if necessary and identify by block number)

A combined source-channel coding approach is described for the encoding, transmission and remote reconstruction of image data. The source encoder employs two-dimensional (2-D) differential pulse code modulation (DPCM). This is a relatively efficient encoding scheme in the absence of channel errors. In the presence of channel errors, however, the performance degrades rapidly. By providing error control protection to those encoded bits which contribute most significantly to image reconstruction, it is possible to minimize this degradation without sacrificing transmission bandwidth. The result is a relatively robust

next page

DD FORM 1 JAN 73 1473 EDITION OF 1 NOV 65 IS OBSOLETE
S/N 0102-014-6601

Unclassified

SECURITY CLASSIFICATION OF THIS PAGE(When Data Entered)

design which is reasonably insensitive to channel errors and yet provides performance approaching the rate-distortion bound. Analytical results are provided for assumed 2-D autoregressive image models while simulation results are described for real-world images.

SECURITY CLASSIFICATION OF THIS PAGE(When Data Entered)